ARTICLE

Dynein regulates Kv7.4 channel trafficking from the cell membrane

Jennifer van der Horst[1], Salomé Rognant[1] , Geoffrey W. Abbott[2] , Lijo Cherian Ozhathil[1] , Per Hägglund[1] , Vincenzo Barrese[3,4], Christine Y. Chuang[1], Thomas Jespersen[1], Michael J. Davies[1] , Iain A. Greenwood[3], Pontus Gourdon[1,5] , Christian Aalkjær[1,6] , and Thomas A. Jepps[1]

The dynein motor protein transports proteins away from the cell membrane along the microtubule network. Recently, we found the microtubule network was important for regulating the membrane abundance of voltage-gated Kv7.4 potassium channels in vascular smooth muscle. Here, we aimed to investigate the influence of dynein on the microtubule-dependent internalization of the Kv7.4 channel. Patch-clamp recordings from HEK293B cells showed Kv7.4 currents were increased after inhibiting dynein function with ciliobrevin D or by coexpressing p50/dynamitin, which specifically interferes with dynein motor function. Mutation of a dynein-binding site in the Kv7.4 C terminus increased the Kv7.4 current and prevented p50 interference. Structured illumination microscopy, proximity ligation assays, and coimmunoprecipitation showed colocalization of Kv7.4 and dynein in mesenteric artery myocytes. Ciliobrevin D enhanced mesenteric artery relaxation to activators of Kv7.2–Kv7.5 channels and increased membrane abundance of Kv7.4 protein in isolated smooth muscle cells and HEK293B cells. Ciliobrevin D failed to enhance the negligible S-1–mediated relaxations after morpholino-mediated knockdown of Kv7.4. Mass spectrometry revealed an interaction of dynein with caveolin-1, confirmed using proximity ligation and coimmunoprecipitation assays, which also provided evidence for interaction of caveolin-1 with Kv7.4, confirming that Kv7.4 channels are localized to caveolae in mesenteric artery myocytes. Lastly, cholesterol depletion reduced the interaction of Kv7.4 with caveolin-1 and dynein while increasing the overall membrane expression of Kv7.4, although it attenuated the Kv7.4 current in oocytes and interfered with the action of ciliobrevin D and channel activators in arterial segments. Overall, this study shows that dynein can traffic Kv7.4 channels in vascular smooth muscle in a mechanism dependent on cholesterol-rich caveolae.

Introduction

The repertoire of ion channels found in the membrane of any given cell determines the functionality of the cell. Thus, the trafficking of ion channels into and away from the cell membrane must be carefully controlled for the cell to maintain an appropriate physiological response. Ion channels found in the cell membrane will be ultimately internalized and either recycled back into the cell membrane or degraded. In heterologous expression systems, the internalization and overall surface expression of several potassium channels is reported to be influenced by the dynein motor protein, including the voltage-dependent Kv1.5, Kv2.1, and Kv3.1 channels (Choi et al., 2005; Loewen et al., 2009; Steele and Fedida, 2014).

Dynein is a motor protein bound to the microtubule network that transports "cargo," including membrane proteins, along cellular paths created by microtubules. This motor protein complex utilizes ATP hydrolysis to drive retrograde movement toward the minus ends of microtubules, i.e., away from the cell membrane (Franker and Hoogenraad, 2013; Bhabha et al., 2016).

Recently, our laboratory showed that disruption of microtubules (with colchicine and nocodazole) increased the membrane levels and function of the voltage-gated potassium channel Kv7.4 (Lindman et al., 2018). In rat mesenteric and renal arteries, where Kv7.4 channels are important physiologically (Stott et al., 2014; van der Horst et al., 2020), microtubule disruption increased Kv7 channel function, which was associated

with increased Kv7.4 membrane expression in vascular myocytes. The microtubule-dependent mechanisms that orchestrate this novel regulation pathway are yet to be determined.

The aim of this study was to investigate the influence of dynein on the microtubule-dependent trafficking of the Kv7.4 channel. Herein, we show that dynein binds to Kv7.4 channels to regulate their trafficking away from the cell membrane, which has important implications in vascular physiology. Furthermore, we identify the cholesterol-rich domains of caveolae as being important for this process in vascular smooth muscle cells.

Materials and methods

In silico analysis
Human Kv7.1–Kv7.5, encoded by *KCNQ1* to *KCNQ5* genes, respectively (UniProt accession nos. P51787, O43526, O43525, P56696, and Q9NR82) and *Xenopus laevis* Kv7.1 (UniProt accession no. P70057), were aligned using Clustal Omega (Sievers et al., 2011), yielding the full-sequence alignment. We identified similarity to previously identified dynein-binding motifs (Rodríguez-Crespo et al., 2001). The cryo-EM structure of *Xenopus* Kv7.1 (PDB accession no. 5VMS; Sun and MacKinnon, 2017) was visualized using PyMOL (version 1.8; Schrödinger, LLC).

Animals
All animal experiments were performed in accordance with Directive 2010/63EU on the protection of animals used for scientific purposes and were approved by the National Ethics Committee, Denmark. Male Wistar rats were purchased from Janvier Labs, group-housed in clear plastic containers, and underwent at least 1 wk of habituation before use. All experiments were performed using 14–17-wk-old male Wistar rats euthanized by cervical dislocation.

Reagents
Some the main reagents used in this study are listed below.

Ciliobrevins (Tocris) are a group of small molecules that inhibit the motor activity of dynein by acting as ATP competitors for the dynein adenosine triphosphatase, without disturbing dynein binding to microtubules and without affecting other motor proteins, such as kinesin (Firestone et al., 2012; Roossien et al., 2015). These inhibitory effects are observed between 10 and 40 µM (Firestone et al., 2012; Eyre et al., 2014).

Methyl-β-cyclodextrin (M-βCD; Sigma-Aldrich) depletes cholesterol (Kilsdonk et al., 1995) and disrupts caveolae in arterial preparations while maintaining the contractile phenotype at concentrations <10 mM (Dreja et al., 2002).

Filipin III (Sigma-Aldrich) is a polyene antibiotic that forms complexes with cholesterol to reduce its ability to interact with proteins at concentrations <10 µM, as used in this study (Norman et al., 1972; Delgado-Ramírez et al., 2018).

S-1 and NS15370 (kind gift from NeuroSearch, Ballerup, Denmark) are activators of Kv7.2–Kv7.5 channels with no effect on Kv7.1 channels. At the concentrations used in this study, the effects of these compounds can be fully prevented by Kv7 blockers, such as XE991 or linopirdine (Bentzen et al., 2006; Dalby-Brown et al., 2013; Chadha et al., 2014; Jepps et al., 2014).

Plasmid construction and site-directed mutagenesis
Human KCNQ4 was subcloned into the mammalian expression vector pEGFP-N2 (GenBank accession no: U57608), with the gene cloned into a pEGFP-N2 vector so that it is in frame with the enhanced GFP (EGFP) coding sequences, enabling the expression of KCNQ4 as fusion to the N terminus of EGFP. Mutant KCNQ4 cDNA was generated by PCR-based site-directed mutagenesis using the Quick Change II Site-Directed Mutagenesis Kit (Agilent Technologies). Human p50 (Dynamitin/DCTN2) in pCMV3 was purchased from Sino Biological (HG14449-UT). Overexpression of p50 in HEK293B cells was used as a tool to disrupt the dynein motor system by dissociating the dynactin complex, a complex required for dynein activity (Echeverri et al., 1996; Schroer, 2004; Loewen et al., 2009).

HEK293B cell culture and transfection
HEK293B cells were cultured to 80% confluency before passaging and used for experimentation between P10 and P30. Cells were grown in Dulbecco's modified Eagle's medium (DMEM) containing, glutamax, 1% penicillin/streptomycin, and 10% FBS (Substrate Department, the Panum Institute) in an incubator with 5% CO_2. For proximity ligation assay (PLA) experiments, 500 µl cell solution was plated on 12-mm coverslips in 24-well plates 1 d before transfection and stored at 37°C with 5% CO_2. The cells on the coverslips were transfected at 60% confluency with 50 ng GFP-tagged Kv7.4 or Kv7.4-Q580A mixed with 0.15 µl Lipofectamine 2000 (Invitrogen) and 40 µl Opti-MEM (GIBCO). The cells were incubated for 24 h at 37°C with 5% CO_2. Cells were used for PLA experiments 24 h after transfection. For Western blotting and coimmunoprecipitation experiments, HEK293B cells were cultured in a T25 flask and transiently transfected with 1 µg GFP-tagged Kv7.4 or Kv7.4-Q580A mixed with 3 µl Lipofectamine 2000 (Invitrogen) and 50 µl Opti-MEM (GIBCO). Cells were harvested 24 h after transfection in radioimmunoprecipitation assay buffer (in mM): 50 Tris, pH 8.0, 150 NaCl, 1% NP-40, 1% SDS, 0.5% sodium deoxycholate, and protease inhibitor cocktail (Roche) or in immunoprecipitation-lysis buffer (in mM): 50 Tris, pH 8.5, 5 EDTA, 150 NaCl, 10 KCl, 1% Nonidet P40, and protease inhibitor cocktail (Roche) and used for Western blotting or coimmunoprecipitation experiments, respectively.

Electrophysiology
HEK293B cells, cultured at 37°C in DMEM supplemented with 10% FBS and 4 mM glutamine, were transiently transfected with 1 µg EGFP-tagged Kv7.4 or Kv7.4-Q580A in a T25 flask mixed with 3 µl Lipofectamine 2000 (Invitrogen) and 50 µl Opti-MEM (GIBCO). Kv7.4 and Kv7.4-Q580A were coexpressed with 1 µg p50/dynamitin (catalog: HG14449-UT; SinoBiological). The cells were incubated for 24 h at 37°C with 5% CO_2. Cells were used 24 h after transfection.

Electrophysiological recordings were performed in whole-cell patch-clamp configuration with patch pipettes pulled from 1.5-mm borosilicate glass capillaries (World Precision Instruments, Inc.) using micropipette puller P97 (Sutter Instruments Co.). Pipette tips were polished to have a pipette resistance of 4–6 MΩ in the bath solution. The pipette solution contained (in

van der Horst et al.
Dynein regulates Kv7 channels

Journal of General Physiology
https://doi.org/10.1085/jgp.202012760

2 of 19

mM) 110 KCl, 10 EGTA, 5.17 CaCl$_2$, 1.42 MgCl$_2$, 4 K$_2$ATP, and 10 HEPES (pH 7.4 with KOH). The bath solution contained (in mM) 140 NaCl, 4 KCl, 2 CaCl$_2$, 1 MgCl$_2$, 10 HEPES, and 10 glucose (pH 7.4 with NaOH). Whole-cell currents were recorded with a Multiclamp 700B amplifier (Molecular Devices) controlled by Clampex 10 via digidata 1550 (Molecular Devices). Data were low-pass filtered at 5 kHz and sampled at 10 kHz. All the experiments were performed at room temperature (21°C). Stock solutions of ciliobrevin D were prepared in DMSO and diluted to the appropriate concentration (3 µM) in the bath solutions. The cells were incubated with ciliobrevin D for 15 min before recording currents. For I-V relations, currents were recorded using a stimulation protocol consisting of voltage steps of 2 s from holding potential of −80 mV, ranging from −60 to +40 mV. Currents were measured from the end of the 2-s voltage step and were normalized to the cell capacitance. Steady-state activation curves were constructed by dividing the steady-state current at each voltage to the maximum current at +40 mV. To calculate $V_{1/2}$ for each given condition, the steady-state activation curves were fitted with a Boltzmann equation.

All analyses and preparation of the figures were done in Igor Pro 6 (WaveMetrics Inc.).

In silico docking

The ciliobrevin D molecule was docked in silico to the human Kv7.1 (Sun and MacKinnon, 2020) and human Kv7.4 (Li et al., 2021) cryo-EM structures that were available at the time of writing. Mutant channels were created by substitution in UCSF Chimera. The unguided docking was performed with CHARMM force fields (Grosdidier et al., 2011a) using SwissDock (Grosdidier et al., 2011b).

Immunoprecipitation and Western blotting

For immunoprecipitation experiments using rat mesenteric artery lysate, three animals' worth of mesenteric arteries were pooled for protein extraction and homogenized in 200 µl lysis buffer (in mM): 50 Tris, pH 8.5, 5 EDTA, 150 NaCl, 10 KCl, 1% Nonidet P40, and protease inhibitor cocktail (Roche) for 10 min at 4°C. After centrifugation at 11,000 g for 10 min at 4°C to remove cell debris, the supernatant was collected followed by protein quantitation using a bicinchoninic acid Protein Assay kit (Thermo Fisher Scientific). For immunoprecipitation of heterologously expressed Kv7.4, HEK293B cells were maintained in DMEM supplemented with 10% FBS and 1% penicillin-streptomycin. Transient DNA transfections were performed with Lipofectamine using 1 µg Kv7.4 plasmid DNA/T25 flask. The transfected HEK293B cells were harvested 24 h after transfection by centrifugation, and then the cell pellet was incubated on ice for 30 min with 200 µl lysis buffer. After centrifugation at 11,000 g for 10 min at 4°C, the supernatant was collected followed by protein quantitation using a bicinchoninic acid Protein Assay kit (Thermo Fisher Scientific).

Total cell protein lysate was immunoprecipitated using a Dynabeads Protein G Immunoprecipitation Kit (Thermo Fisher Scientific). Briefly, 1.5 mg magnetic dynabeads were transferred to 1.5-ml tubes and placed on a magnet to separate the beads from the solution. The supernatant was removed, and the beads

were resuspended with 3 µg anti-dynein antibody (ab23905; Abcam) or anti–caveolin-1 antibody (C3237; Sigma-Aldrich) diluted in 200 µl antibody binding buffer. Tubes containing Dynabeads–Ab complex were incubated with rotation for 30 min at 21°C and placed on a magnet to remove the supernatant. After the Dynabeads–Ab complex was washed in Ab binding and washing buffer, the supernatant was removed, and the Dynabeads–Ab complex was resuspended with 1 mg total rat mesenteric artery protein lysate or 50 µg HEK cell lysate in 200 µl PBS (pH 7.4) and incubated with rotation overnight at 4°C. Subsequently, the Dynabeads–Ab–Ag complex was washed three times in PBS; thereafter, the supernatant was removed, and the Dynabeads–Ab–Ag complex was denatured at 70°C for 10 min in the presence of 20 µl elution buffer (50 mM glycine, pH 2.8), NuPAGE sample buffer, and reducing agent (Thermo Fisher Scientific) to elute Ab–Ag complex from the beads. Samples of the total supernatant were then loaded onto SDS-PAGE gels (4–12% bis–tris; Invitrogen), subjected to electrophoresis, and then transferred onto a polyvinylidene fluoride membrane (Immobilon-FL; Sigma-Aldrich). The membrane was probed with an anti-dynein (1:1,000; ab23905; Abcam), anti–caveolin-1 (1:2,000; C3237; Sigma-Aldrich), anti-Kv7.4 (1:200; sc-50417; Santa Cruz Biotechnology), or anti-GFP (1:2,000; A-11122; Thermo Fisher Scientific) antibody. Protein bands were visualized using fluorescently conjugated secondary antibodies raised in mouse and rabbit (both at 1:10,000; Li-Cor Biosciences) and imaged and analyzed on the Odyssey Infrared Imaging System (Li-Cor Biosciences; version 5.2.5).

Mass spectrometry (MS)

Immunoprecipitated samples eluted from Dynabeads (see above) were subjected to trypsin digestion following the filter-aided sample preparation procedure (Wiśniewski et al., 2009). Briefly, samples were diluted in 8 M urea and 0.1 M Tris, pH 8.5, to 500 µl, and then concentrated on Vivaspin 500 ultrafiltration devices (Sartorius) at 14,000 g (21°C) to a volume of <20 µl. Following addition of 400 µl of 40 mM dithiothreitol in 8 M urea, 0.1 M Tris, pH 8.5, samples were incubated at 21°C for 30 min and centrifuged as above. Samples were then treated with 400 µl of 50 mM iodoacetamide in 8 M urea and 0.1 M Tris, pH 8.5, and incubated for 30 min at 21°C in the dark. The samples were then centrifuged as above before 8 M urea and 0.1 M Tris, pH 8.0, was added (repeated twice). Finally, the samples received 400 µl of 1.6 M urea in 0.1 M Tris, pH 8.0, and were centrifuged to a volume of <20 µl followed by the addition of 100 µl of 1.6 M urea in 0.1 M Tris, pH 8.0, and 1 µl sequence grade trypsin (Promega; 0.1 µg/µl). Following overnight incubation (21°C), samples were centrifuged as above, and the flow through was subjected to solid-phase extraction on Empore C18 discs, as described previously (Rappsilber et al., 2003). Peptide samples were analyzed on an Impact II Q-TOF mass spectrometer (Bruker) coupled to a Dionex Ultimate 3000RSnano chromatography system (Thermo Fisher Scientific). Peptides were loaded onto a Nanoelute C18 column (75 µm × 15 cm, 1.9-µm particle size; Bruker) and eluted over 65 min using a gradient elution system consisting of mobile phase A (0.1% formic acid in H$_2$O) and B (80% acetonitrile in H$_2$O containing 0.1% formic

acid) at a flow rate of 0.3 µl/min. The mass spectrometer was operated with cycles of a MS scan followed by up to 12 tandem MS scans of the most intense precursor ions. MaxQuant version 1.6.1.0 (www.maxquant.org) was used as a database search engine for identification of peptides with the following parameters: carbamidomethylation of Cys (fixed modification); Met oxidation and N-terminal acetylation (variable modifications); allowed number of missed cleavages, two; first search mass tolerance, 0.07 D; and main search mass tolerance, 0.006 D. The output data were filtered to exclude proteins that did not match the acceptance criteria of at least two confidently matched peptides in four out of four replicates, which were absent in control samples from immunoprecipitations without IgG and in the presence of normal mouse control IgG.

Immunocytochemistry
Freshly isolated rat mesenteric artery myocytes were isolated as previously described (Jepps et al., 2015). Briefly, dissected mesenteric arteries were placed in smooth muscle dissection solution (SMDS) containing (in mM) 60 NaCl, 80 sodium glutamate, 5 KCl, 2 $MgCl_2$, 10 glucose, and 10 HEPES, pH 7.4, at 37°C for 10 min. Mesenteric arteries were then placed in SMDS containing BSA, papain, and dithiothreitol for 8 min at 37°C, before being washed several times in ice-cold SMDS and incubated again at 37°C in SMDS containing calcium, BSA, collagenase type F, and collagenase type H. Following several washes in ice-cold SMDS, the tissue was triturated gently with a glass pipette. Cells were allowed to adhere to coverslips, then fixed in 4% paraformaldehyde in PBS at 21°C for 30 min and incubated with a blocking solution consisting of 0.2% fish skin gelatin in PBS containing 0.1% Triton X-100 (PBST). Cells were then incubated with primary antibodies diluted in PBST overnight at 4°C. Primary antibodies used were Kv7.4 (1:200; ab65797; Abcam), dynein (1:500; ab23905; Abcam), β-tubulin (1:500; A1126; Invitrogen) and caveolin-1 (1:500; ab17052; Abcam), and sodium-calcium exchanger (NCX; 1:500; R3F1; Swant). Cells were visualized with structured illumination microscopy using a Zeiss Elyra PS.1 Super Resolution Microscope (Carl Zeiss). Cells stained with the NCX antibody were visualized using a Carl Zeiss LSM900 Confocal Super Resolution Microscope with Airyscan 2. Midcell xy sections were selected and analyzed. Total cell fluorescence and intracellular fluorescence signals were quantified using Zen 2012 confocal software.

In a subset of experiments, HEK293B cells transfected with Kv7.4-EGFP (as described above) were allowed to adhere to coverslips, the nuclei were stained with 4′,6-diamidino-2-phenylindole (Thermo Fisher Scientific), and the cells were visualized on an LSM780 confocal microscope (Carl Zeiss).

PLA
Colocalization of dynein with Kv7.4 or caveolin-1 and caveolin-1 with Kv7.4 was studied with PLA in HEK293B cells stably expressing Kv7.4 and Kv7.4-Q580A or freshly isolated rat mesenteric artery myocytes using the Duolink in situ (PLA) detection kit 563 (Olink) per the manufacturer's instructions. Similar to previous studies (Zhong et al., 2010a; Brueggemann et al.,

2014; Chadha et al., 2014; Jepps et al., 2015; Stott et al., 2016; Barrese et al., 2020), cells were allowed to adhere to coverslips and fixed in 4% paraformaldehyde in PBS. Cells were permeabilized in PBST, blocked in Duolink blocking solution, and incubated with pairs of primary antibodies. The primary antibodies employed were dynein (ab23905; Abcam), Kv7.4 (ab65797; Abcam), caveolin-1 (1:500 ab17052; Abcam), caveolin-1 (C3237; Sigma-Aldrich), and NCX (R3F1; Swant). Combinations of secondary anti-rabbit or anti-mouse antibodies of PLA PLUS and MINUS probes were used followed by hybridization, ligation, and amplification steps. Colocalization signals (proteins located within 40 nm of each other) were visualized with a standard Zeiss LSM710 upright laser-scanning confocal microscope.

Myography
Third-order branches of rat mesenteric artery were removed from the animals and cleaned of adherent tissue in physiological salt solution (PSS) containing (in mM) 121 NaCl, 2.8 KCl, 1.6 $CaCl_2$, 25 $NaHCO_3$, 1.2 KH_2PO_4, 1.2 $MgSO_4$, 0.03 EDTA, and 5.5 glucose. Following dissection, vessels were cut into 2-mm segments and mounted in a wire myograph (Danish Myo Technology) for isometric tension recordings. The chambers of the myograph contained PSS maintained at 37°C and aerated with 95% O_2/5% CO_2. Changes in tension were recorded continuously by PowerLab and Chart software (ADInstruments). Arterial segments were equilibrated for 30 min and normalized to passive force (Mulvany and Halpern, 1977). Subsequently, the arteries were contracted with 10 µM of α_1-adrenergic receptor agonist methoxamine to assess viability. The chambers were washed with PSS before artery segments were incubated with or without 10 µM ciliobrevin D, 5 mM M-βCD for 1 h, or 3 µM Filipin III for 30 min. After incubation, the arteries were precontracted with 10 µM methoxamine. Subsequently, Kv7.2–Kv7.5 specific activators S-1 (0.1 µM–10 µM) or NS15370 (1 nM–1 µM) were applied to the arteries cumulatively.

Morpholino transfections
To determine the functional impact of Kv7.4 channels in the ciliobrevin D–enhanced vasorelaxations, we employed a morpholino-induced Kv7.4 knockdown technique that was shown previously to efficiently knock down Kv7.4 channels in rat mesenteric arteries (Jepps et al., 2015; Stott et al., 2018). We transfected whole mesenteric artery segments with either a Kv7.4-targeted morpholino or a miss-match control morpholino (with five bases altered from the targeted sequence). Morpholino oligonucleotides (100 nM; Gene Tools Inc.) were mixed with Lipofectamine 2000 (Life Technologies) in Opti-MEM and left at 21°C for 2 h. The Opti-MEM mix was then added to DMEM containing HEPES, glutamax, and $NaHCO_3$ (Substrate Department, the Panum Institute), and the third-order mesenteric arteries were placed in this solution at 37°C. After 36 h of incubation, arteries transfected with miss-match or Kv7.4-targeted morpholino were mounted in the wire myograph for isometric tension recordings, and viability was tested using 20 µM methoxamine. This technique was used due to a lack of a Kv7.4-specific inhibitors.

Two-electrode voltage clamp (TEVC)

Complimentary RNA (cRNA) encoding human Kv7.4 was generated by in vitro transcription using the T7 polymerase mMessage mMachine kit (Thermo Fisher Scientific) after linearization of a vector incorporating *Xenopus* β-globin 5′ and 3′ untranslated regions flanking the human KCNQ4 coding region to enhance translation and cRNA stability. We quantified cRNA by spectrophotometry. Defolliculated stage V and VI *Xenopus* oocytes (Xenoocyte) were injected with Kv7.4 cRNA (10 ng total per oocyte). Oocytes were incubated at 16°C in Barth's saline solution containing penicillin and streptomycin and were washed daily for 3 d before TEVC recording. TEVC was performed at room temperature using an OC-725C amplifier (Warner Instruments) and pClamp11 software (Molecular Devices). For recording, oocytes were placed in a small-volume oocyte bath (Warner Instruments) and viewed with a dissection microscope. Chemicals were sourced from Sigma Aldrich. Bath solution was (in mM) 96 NaCl, 4 KCl, 1 MgCl$_2$, 1 CaCl$_2$, and 10 HEPES, pH 7.6. M-βCD was prepared fresh in bath solution each experimental day and introduced into the oocyte recording bath by gravity perfusion at a constant flow of 1 ml per minute for at least 3 min before recording. Pipettes were of 1–2 MΩ resistance when filled with 3 M KCl. We recorded currents in response to voltage pulses to +40 mV from a holding potential of –80 mV. Electrophysiology data analysis was performed with Clampfit (Molecular Devices) and Origin software (OriginLab Corporation); values are stated as mean ± SEM.

Statistical analysis

All statistical analysis was performed using GraphPad Prism 7. Mean logEC$_{50}$ (half-maximal effective concentration) and maximal relaxation (Rmax) values were calculated from individual experiments and compared by an unpaired *t* test or, when more than two groups were compared, a one-way ANOVA followed by a Sidak or Tukey posttest. When it was not possible to calculate logEC$_{50}$ values, concentration-effect curves were tested with two-way ANOVAs followed by the Bonferroni posttest with correction for multiple comparisons. Membrane expression data were compared with a one-way ANOVA followed by a Tukey posttest or an unpaired *t* test, depending on the number of groups in the comparison. Mean puncta in PLAs were compared by an unpaired *t* test. All data are presented as means ± SEM.

Results

Dynein inhibition enhances Kv7.4 currents in HEK cells

As the dynein motor protein is critical for retrograde microtubule network transport, we investigated whether a dynein-recognition site was present in the Kv7.4 channel protein. Similarity to two established dynein-binding motifs was identified, KSTQT and GIQVDR (Rodríguez-Crespo et al., 2001), separated by a single arginine (R; Fig. 1 A). These sites are located in the intracellular C terminus of the protein at the junction between the so-called C and D helices, distal to the membrane. Further analysis using the structure of the homologous Kv7.1 protein (Howard et al., 2007) suggests that several residues in the equivalent sequence-stretch of Kv7.4, specifically

the underscored residues in K̲S̲L̲Q̲T̲-R̲-V̲D̲QIVG, are accessible to the intracellular environment (Fig. 1 B). The high agreement of these exposed amino acids with the established recognition sites, in particular for the first motif, likely allow contact with dynein and suggest that this interaction is based on charge complementation. We note that the motifs are rather conserved among the Kv7 protein family, suggesting that other Kv7 channel isoforms may also be governed by dynein.

To test the hypothesis that these dynein-recognition sites in Kv7.4 are crucial for the binding of dynein and regulation of the channel, we substituted one of the intracellularly exposed amino acids in the first motif, Q580, with alanine, which is expected to interrupt the channel interaction with dynein. Voltage-clamp electrophysiology experiments on HEK cells overexpressing Kv7.4-Q580A (*n* = 6) showed increased Kv7.4 currents at +30 and +40 mV compared with control Kv7.4 currents (*n* = 10; Fig. 1 C). Coexpression of p50/dynamitin, to interfere with dynein function, increased Kv7.4 currents at voltages positive to 0 mV (*n* = 5) but had no effect on the Kv7.4-Q580A currents (*n* = 6; Fig. 1 C). In addition, a dynein-specific inhibitor, 3 μM ciliobrevin D, enhanced the Kv7.4 currents at voltages positive to 10 mV but inhibited the Kv7.4-Q580A currents (*n* = 5–7; Fig. 1 C). The voltage of half-maximal activation was not affected in the Q580A mutant nor with cotransfection with p50 or ciliobrevin application (Fig. 1 C).

To investigate the inhibition of the Kv7.4-Q580A current by ciliobrevin, we performed in silico docking simulations (Fig. 1 D). For these simulations, we used the known structure of Kv7.1 and the recently published Kv7.4 structure (Sun and MacKinnon, 2020; Li et al., 2021). Ciliobrevin D was unable to bind to the WT Kv7.1 and Kv7.4 channels, whereas both the Kv7.1-Q560A and Kv7.4-Q586A channels allowed ciliobrevin D to bind (Fig. 1 D). In the simulation with Kv7.4, it appears the glutamine (Q580) provides steric hindrance to prevent ciliobrevin D binding, but the smaller alanine in Kv7.4-Q580A allows binding. We suggest that binding of ciliobrevin D to this part of the C terminus would either prevent channel multimerization or forward trafficking of the channel from the ER (Howard et al., 2007; Haitin and Attali, 2008; Wiener et al., 2008), thereby reducing the number of functional channels in the cell membrane, which would result in a reduced current.

Dynein is colocalized with Kv7.4 in HEK293B cells

Western blot analysis showed that the WT Kv7.4 and Kv7.4-Q580A channels were expressed at similar levels in HEK293B cells (Fig. 2 A). PLA experiments showed colocalization of Kv7.4 and dynein in HEK293B cells transfected with Kv7.4. In cells transfected with Kv7.4-Q580A, the number of PLA puncta was reduced, suggesting reduced interaction of dynein with the Kv7.4-Q580A protein (Kv7.4-WT: 15 cells, Kv7.4-Q580A: 20 cells; P < 0.0001; Fig. 2 B).

Dynein is expressed in vascular smooth muscle and colocalizes with Kv7.4

The presence of dynein in rat mesenteric artery lysates was evidenced by Western blotting (Fig. 3 A). Expression of dynein in intact smooth muscle cells was confirmed using structured
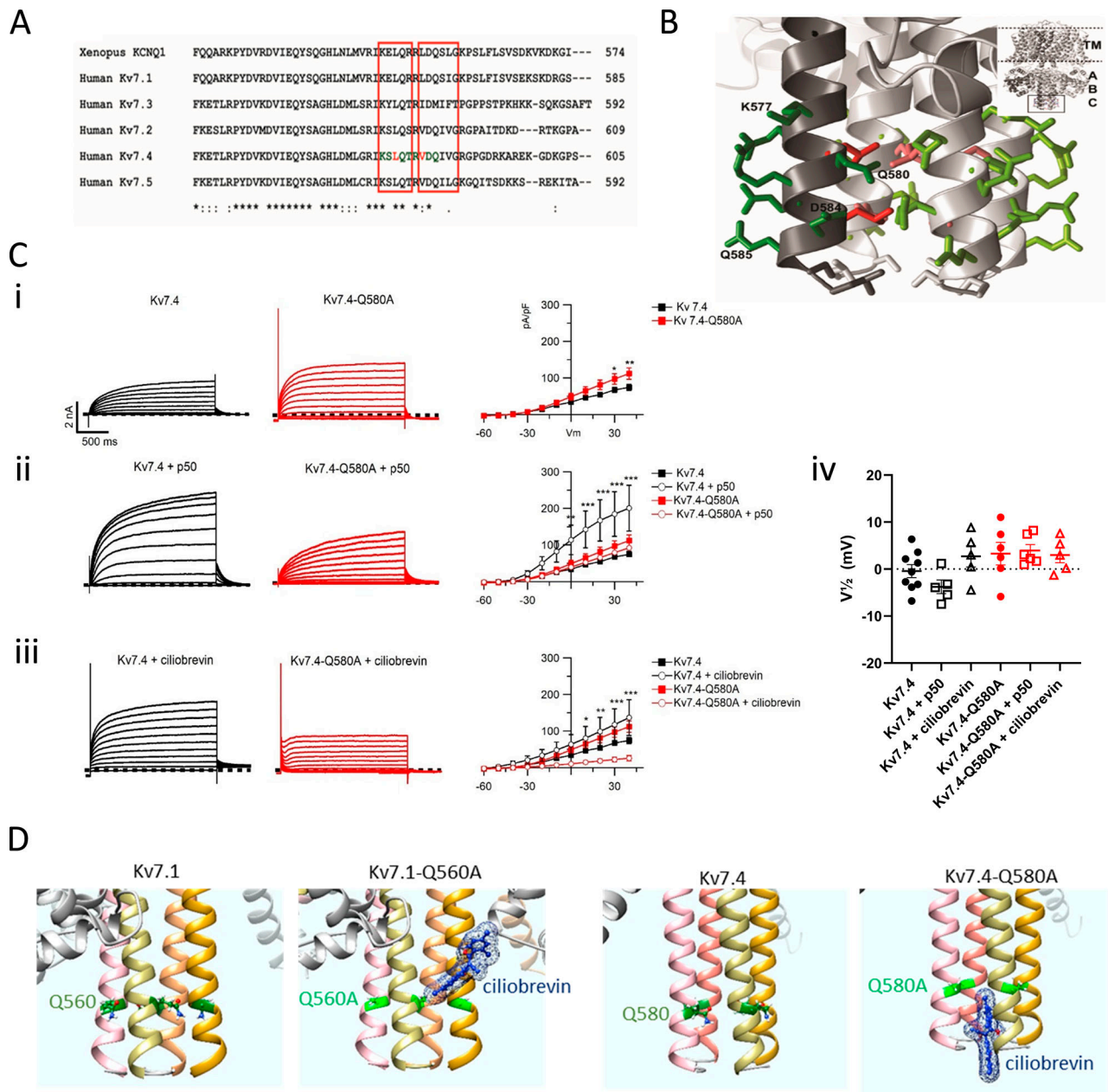
Figure 1. **Dynein binds to the Kv7.4 C terminus. (A)** Amino acid alignment of the end of the c-helix of *Xenopus* Kv7.1 (used for the modeling in B) and human Kv7.1–Kv7.5 channels. **(B)** Close view of the Kv7 channel c-helix using the structure of *Xenopus* Kv7.1 suggests that several residues (highlighted in green) in the dynein-binding motifs indeed are accessible to the intracellular environment. Those in red are not exposed to the intracellular environment and are therefore unlikely to be required for dynein recognition. **(C, i–iii)** Representative whole-cell voltage clamp recordings and respective I-V relations compared between Kv7.4 and Kv7.4-Q580A (i); when cotransfected with p50/dynamitin (ii); or incubation with 3 µM ciliobrevin D (iii). Statistical comparisons were made with a two-way ANOVA, followed by a Bonferroni multiple comparisons test, where $P < 0.05$, $P < 0.01$, and $P < 0.001$ are depicted by *, **, and ***, respectively. **(C iv)** Mean $V_{1/2}$ for steady-state activation was compared for each condition with a one-way ANVOA. **(D)** Docking simulations performed with SwissDock on Kv7.1, Kv7.4, Kv7.1-Q560A, and Kv7.4-Q580A showing ciliobrevin D binding to both mutant channels but neither WT channel. Each of the four spirals (pink, green, orange, and gold) represent an intercellular C terminus of each of the four Kv7 protein α subunits that multimerize to form a functional channel. Mean values are shown with error bars depicting the SEM.

illumination microscopy, which showed dynein expression throughout freshly isolated mesenteric artery smooth muscle cells (Fig. 3 B).

Before investigating whether Kv7.4 coimmunoprecipitated with dynein in rat mesenteric artery protein lysate, we confirmed that Kv7.4 is associated directly with dynein in HEK cells.

Immunoprecipitation with an anti-dynein antibody followed by a Western blot using a GFP antibody showed an interaction between dynein and Kv7.4 in HEK293B cells transfected with Kv7.4 (*n* = 3; Fig. 3 C). Having established that this technique allows for coimmunoprecipitation of these two proteins, we identified Kv7.4 protein in rat mesenteric artery lysate
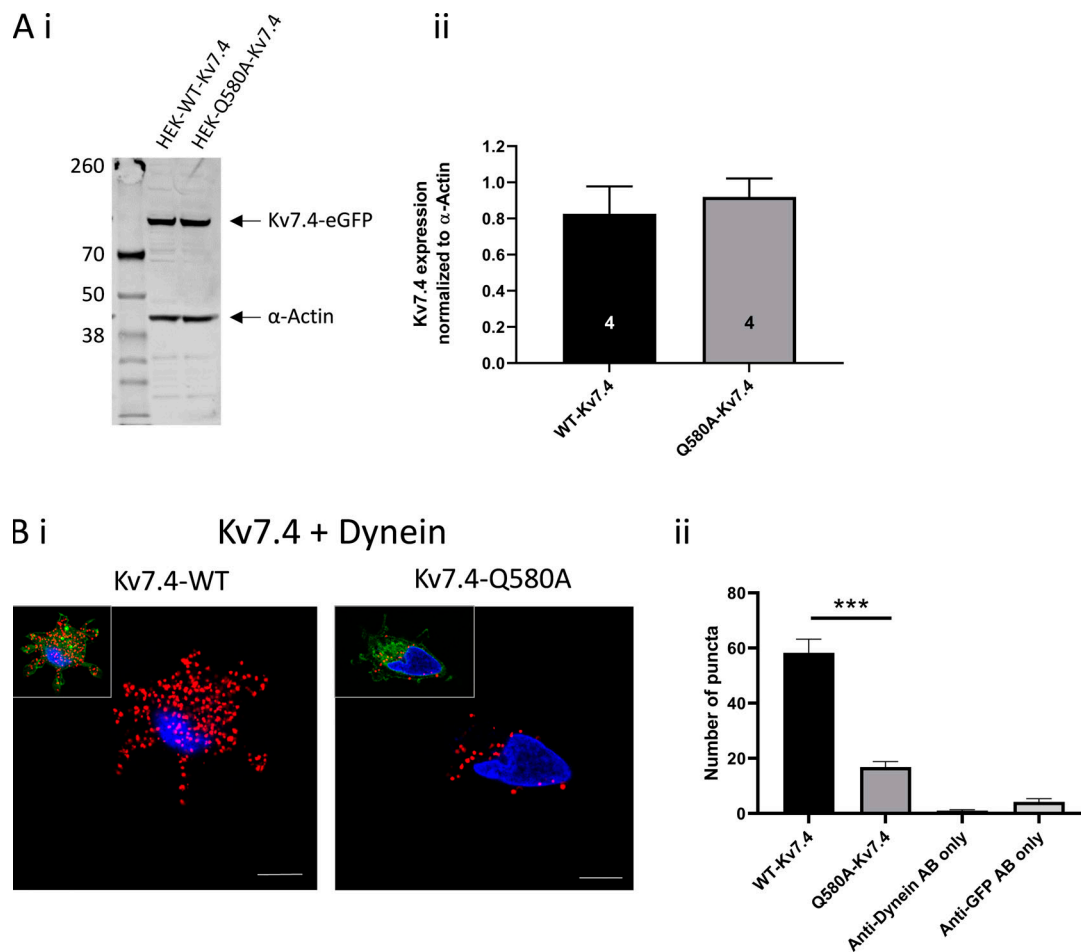
Figure 2. **The Kv7.4-Q580A mutant is less able to bind dynein. (A i)** Representative Western blot with HEK293B cells transfected with WT-Kv7.4-EGFP or Q580A-Kv7.4-EGFP showing Kv7.4-EGFP bands (∼104 kD). **(A ii)** Mean data comparing the Kv7.4-EGFP band intensity in the lysates from HEK293B cells transfected with WT-Kv7.4-EGFP or Q580A-Kv7.4–EGFP. **(B i)** Representative images of PLAs in HEK293B cells transfected with Kv7.4 (left) or Kv7.4-Q580A (right) using Kv7.4 and dynein antibodies. The EGFP is visualized (green) in the insets to show Kv7.4 expression. Each red punctum is representative of the Kv7 channel and dynein protein localizing within 40 nm of one another. **(B ii)** Quantification of puncta in HEK293B cells (Kv7.4-WT: 15 cells, Kv7.4-Q580A: 20 cells) with Kv7.4 and dynein and the respective antibodies alone as control, according to an unpaired t test. ***, P < 0.0001. Scale bars, 5 µm. Mean values are shown with error bars depicting the SEM.

immunoprecipitated with an anti-dynein antibody (n = 3; Fig. 3 D).

Structured illumination microscopy showed the respective localization of dynein and Kv7.4 in freshly isolated mesenteric artery smooth muscle cells (Fig. 3 E). Colocalization (within 40 nm) between dynein and Kv7.4 in freshly isolated mesenteric artery smooth muscle cells was revealed by PLA (34 cells; n = 4 rats; Fig. 3 F). Taken together, these results show dynein colocalizes with Kv7.4 in isolated rat small mesenteric artery myocytes.

Kv7 channel function is enhanced after dynein inhibition

Enhancing Kv7 channels leads to membrane hyperpolarization, thereby reducing the open probability of voltage-dependent calcium channels relaxing precontracted arteries. Activators of Kv7.2–Kv7.5 channels, such as S-1 and NS15370, elicit vasorelaxations, which can be fully prevented by Kv7 blockers such as XE991 or linopirdine (Bentzen et al., 2006; Dalby-Brown et al., 2013; Chadha et al., 2014; Jepps et al., 2014). Using these

pharmacological tools, we identified the functional role of dynein by incubating freshly isolated mesenteric artery segments with the specific dynein inhibitor ciliobrevin D and stimulating the precontracted arteries with increasing concentrations of the Kv7.2–Kv7.5 activator NS15370. Incubation with 10 µM ciliobrevin D increased the relaxation to NS15370 in vessels precontracted with methoxamine (n = 4 or 5; EC$_{50}$ P = 0.0048; Fig. 4, A and B). We also tested an additional Kv7 channel activator, S-1, and found that ciliobrevin D (n = 4) was able to enhance the S-1–mediated relaxation (control n = 7; EC$_{50}$ P = 0.0278; Fig. 4 C). Incubation with ciliobrevin D had no effect on the initial contractions induced by methoxamine (data not shown).

To inhibit Kv7.4 channels specifically, we knocked down Kv7.4 protein in isolated mesenteric arteries using a targeted morpholino to block its translation (Jepps et al., 2015). Functional confirmation of Kv7.4 knockdown was observed in vessels transfected with the Kv7.4-targeted morpholino, where the response to S-1 (1 µM) was inhibited compared with the missmatch control (n = 5; P = 0.01; Fig. 4 D). S-1 relaxation was
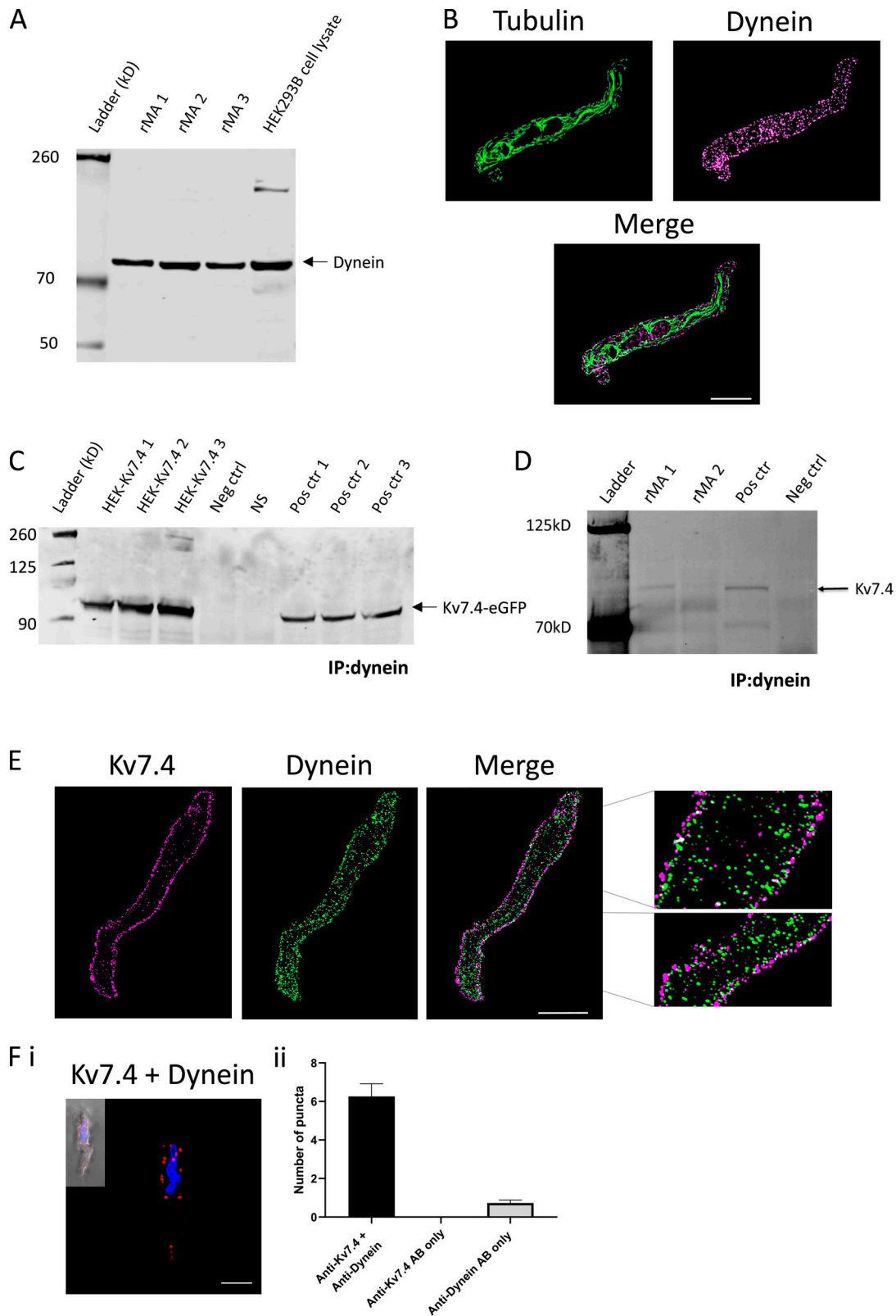
Figure 3. **Dynein colocalizes with Kv7.4 proteins in vascular smooth muscle cells. (A)** Representative Western blot showing dynein (~74 kD) expression in protein lysates from three different samples of rat small mesenteric artery (rMA) and in one protein lysate from untransfected HEK293B cells. **(B)** Representative structured illumination microscopy images of an isolated smooth muscle cell from a rat small mesenteric artery, stained with antibodies against β-tubulin (green) and dynein (magenta). Scale bar, 10 μm. **(C)** Representative Kv7.4 bands from a Western blot following coimmunoprecipitation of dynein in HEK293B cells overexpressing Kv7.4. No bands were detected for the nonspecific binding sample (NS) or for the negative control sample (Neg ctr), where normal mouse control IgG was used instead of the specific pulldown antibody. **(D)** Representative Kv7.4 bands from a Western blot with samples of rat

mesenteric artery protein lysate (rMA) that were immunoprecipitated (IP) with a dynein antibody. Each rMA sample contains n = 3 rats' worth of mesenteric arteries. **(E)** Representative structured illumination microscopy image of an isolated smooth muscle cell from a rat small mesenteric artery stained with antibodies against Kv7.4 (magenta) and dynein (green). Scale bar, 10 μm. **(F i)** Representative image of PLAs with Kv7.4 and dynein antibodies in mesenteric artery myocytes. Each red punctum is representative of the Kv7 channel and dynein protein localizing within 40 nm of one another. **(F ii)** Quantification of puncta in 34 cells (n = 4 rats) with Kv7.4 and dynein and the respective antibodies alone as control. Mean values are shown with error bars depicting the SEM.

enhanced significantly in miss-match control arteries by cilio-brevin D (n = 5; Rmax 74.8 ± 7.2%; P = 0.009), whereas morpholino-induced knockdown of Kv7.4 prevented ciliobrevin D from enhancing S-1–mediated relaxation (Fig. 4 D). Thus, ciliobrevin D is unable to enhance S-1 relaxation in the absence of Kv7.4 channels.

Next, we determined whether ciliobrevin D increased the membrane abundance of Kv7.4 channels in isolated mesenteric myocytes. Fig. 5 A shows that incubation with 3 μM ciliobrevin D increased the expression of Kv7.4 channels in the plasma membrane, relative to the total cell expression (n = 9; P = 0.002). As a control, we investigated whether the expression of the NCX was affected by ciliobrevin D treatment. In these experiments, ciliobrevin D had no effect of the location of the NCX in mesenteric artery smooth muscle cells (n = 10 or 11; Fig. 5 A). We confirmed the ciliobrevin-induced increase of Kv7.4 membrane expression in HEK293B cells (Fig. 5 B). In these experiments, 3 μM ciliobrevin D increased Kv7.4 membrane expression (P = 0.0026). The ciliobrevin D–induced increase in Kv7.4 membrane expression was similar to the effect of 100 μM colchicine treatment (n = 6 or 7; P < 0.001; Fig. 5 B), which we reported previously (Lindman et al., 2018).

Dynein is associated with caveolae proteins

We wanted to investigate whether dynein targeted particular vesicles in vascular smooth muscle to create a better understanding of how Kv7.4 is removed by dynein from the cell membrane. Thus, we performed mass spectrometry on dynein immunoprecipitates from rat mesenteric artery lysate. We were unable to identify Kv7.4 as a positive hit in the dataset, with this likely due to the low abundance of Kv7.4 protein. However, we identified caveolin-1 as well as caveolae-associated protein 1 (cavin-1; n = 4; Table 1) as proteins interacting with dynein, suggesting that dynein binds to proteins forming the caveolae microdomains in the cell membrane.

To verify this interaction, we performed coimmunoprecipitation assays with rat mesenteric artery lysate using antibodies for dynein and caveolin-1. Dynein was identified in the caveolin-1 immunoprecipitate (Fig. 6 A), and in the reverse experiment, caveolin-1 was identified in the dynein immunoprecipitate (Fig. 6 B). To further validate this interaction, we performed PLA with antibodies against dynein and caveolin-1. Fig. 6 C shows PLA puncta were detected with the dynein- and caveolin-1–specific antibodies. Cholesterol depletion with M-βCD reduced the number of interactions between dynein and caveolin-1 (Fig. 6 C; P = 0.004).

Kv7.4 channels are found in caveolae

It is not known if Kv7.4 channels localize in cholesterol-rich regions such as caveolae. To investigate whether Kv7.4

channels are localized to the cholesterol-rich caveolae, we performed structured illumination microscopy on freshly isolated mesenteric artery smooth muscle cells and found Kv7.4 channels to be closely localized with caveolin-1 (Fig. 7 A). To determine colocalization between caveolin-1 and Kv7.4 channels, we performed PLA, which showed that these proteins were localized within 40 nm in smooth muscle cells (27 cells, n = 3 rats; Fig. 7 B). When we incubated rat mesenteric artery myocytes with M-βCD, there was a decrease in the number of associations between caveolin-1 and Kv7.4 (29 cells, n = 3 rats; P = 0.008; Fig. 7 B). For a control interaction with caveolin-1, we also tested whether the NCX protein colocalized with caveolin-1 and if any interaction was affected by cholesterol depletion. Similar to Kv7.4, the NCX colocalized with caveolin-1, but unlike Kv7.4, this interaction was not affected by M-βCD treatment (Fig. 7 C). Overall, these data show colocalizations between Kv7.4 and caveolin-1 proteins, which are dependent on cholesterol, suggesting at least some of the Kv7.4 channels found in the cell membrane are localized in caveolae of vascular smooth muscle cells.

Dynein trafficking of Kv7.4 is dependent on cholesterol

Dynein has been reported to cluster in cholesterol-rich microdomains. Therefore, we tested whether cholesterol depletion reduced the interaction of Kv7.4 with dynein. In mesenteric artery smooth muscle cells, PLA with antibodies against Kv7.4 and dynein showed a reduced number of interactions following M-βCD treatment compared with control (18–20 cells, n = 3 rats; P < 0.0001; Fig. 8 A). Structured illumination microscopy showed that Kv7.4 membrane expression was increased following M-βCD treatment (n = 8–10 cells; P = 0.0001; Fig. 8 B), which was similar to the increase observed with ciliobrevin D treatment. As a control, we observed that the membrane expression of the NCX was unaffected by M-βCD treatment (Fig. 8 B).

Cholesterol depletion inhibits Kv7 channel function in mesenteric arteries

To determine the effect of cholesterol depletion on Kv7.4 currents, we performed TEVC experiments on oocytes over-expressing Kv7.4. Application of 1 mM M-βCD inhibited the Kv7.4 current at 40 mV in four out of five oocytes (P = 0.0029; Fig. 9 A). Incubation of rat mesenteric arteries with M-βCD inhibited NS15370 relaxation (n = 8–14; EC$_{50}$ P < 0.0001; Fig. 9, B and C). Saturation of M-βCD with cholesterol restored the vasodilation to NS15370 (n = 5; Fig. 9, B and C). Interestingly, ciliobrevin D was unable to enhance the NS15370 relaxation in the presence of M-βCD (n = 6; Fig. 9, B and C). To confirm the effect of cholesterol depletion on Kv7 channel function in arteries, we also tested Filipin III. Similar to M-βCD, Filipin III inhibited
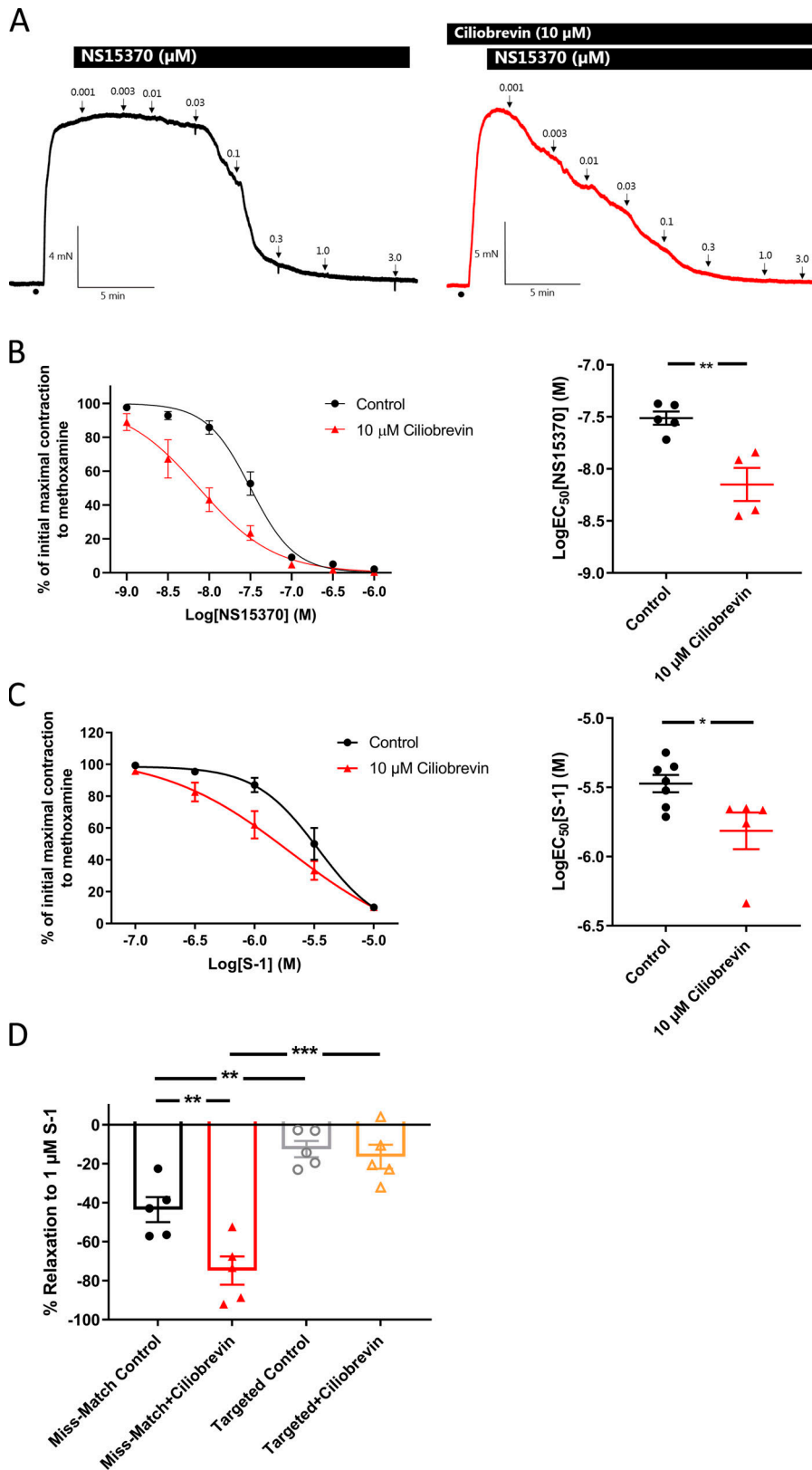
Figure 4. **Kv7 channel function is enhanced following dynein inhibition. (A)** Representative isometric tension recordings of rat mesenteric artery segments preconstricted with methoxamine (•) before sequentially increasing concentrations of Kv7.2–Kv7.5–specific activator NS15370 were applied in control (left) and ciliobrevin D–treated (right) arteries. **(B)** Mean concentration-effect curves and EC_{50} values to the Kv7.2–Kv7.5–specific activator NS15370 showing the effect of NS15370 in rat mesenteric artery segments before and after 10 µM ciliobrevin D incubation. Mean EC_{50} values were compared according to an unpaired t test. **, $P < 0.01$. **(C)** 10 µM ciliobrevin D enhanced the relaxation to another Kv7.2–Kv7.5 channel activator, S-1, according to an unpaired t test. *, $P < 0.05$. **(D)** Rat mesenteric arteries were transfected with either a Kv7.4-targeted or the control (miss-match) morpholino. Relaxations to S-1 were inhibited in arteries transfected with the Kv7.4-targeted morpholino compared with arteries transfected with the control morpholino. Ciliobrevin D enhanced relaxations to S-1 in control arteries, but ciliobrevin D was unable to enhance S-1–mediated relaxation in Kv7.4 knockdown arteries. A one-way ANOVA followed by a Sidak multiple comparisons test was performed, with ** and *** denoting $P < 0.01$ and $P < 0.001$, respectively. Error bars show the mean and SEM.

NS15370 relaxation in rat mesenteric artery segments ($n = 7$; EC_{50} $P = 0.0078$; Fig. 9 D). Taken together, these experiments suggest that arterial Kv7 channels require cholesterol to maintain their normal function.

Discussion

Our laboratory showed previously that microtubule disruption enhanced Kv7 channel–dependent vasorelaxation, which was mediated by an increase in Kv7.4 channel levels in the membrane
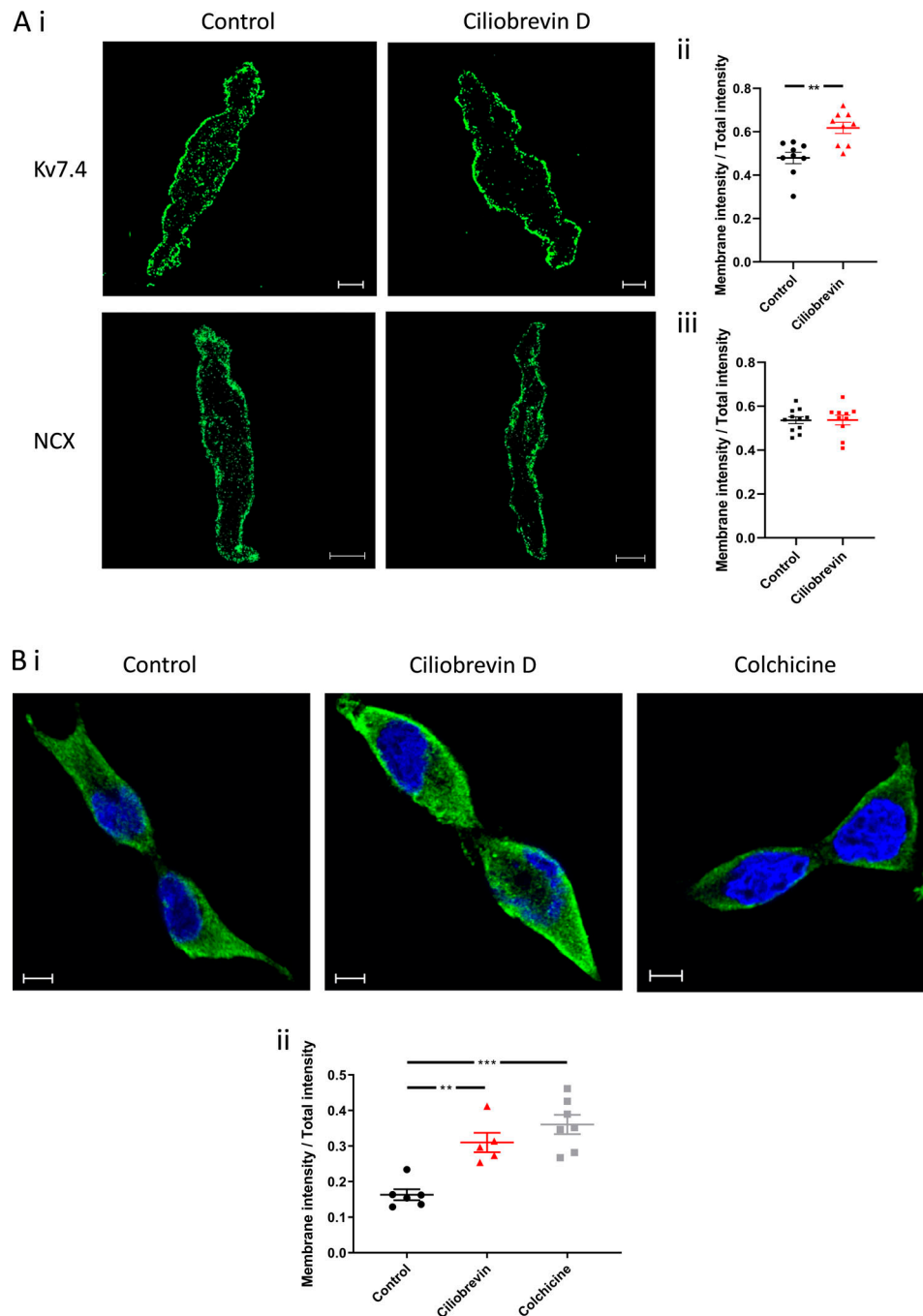
van der Horst et al.
Dynein regulates Kv7 channels

Journal of General Physiology   10 of 19
https://doi.org/10.1085/jgp.202012760

Figure 5. **Dynein inhibition increases membrane expression of Kv7.4 protein. (A, i–iii)** Representative midcell z-section of a mesenteric artery myocyte treated with or without ciliobrevin D and stained for Kv7.4 (top) or NCX (bottom; i). Scale bars, 10 µm. Mean membrane intensity of Kv7.4 (n = 9; ii) and NCX (n = 10 or 11; iii) relative to total intensity in cells treated with ciliobrevin D compared with nontreated cells, calculated from midcell z section. Significance was determined by an unpaired t test. **, P < 0.001. **(B i)** Representative midcell z section of HEK293B cells transfected with Kv7.4-EGFP (green) in nontreated and ciliobrevin D– or colchicine-treated cells. The nuclei are stained with 4′,6-diamidino-2-phenylindole (blue). Scale bars, 10 µm. **(B ii)** Mean membrane intensity of Kv7.4 relative to total intensity in cells treated with ciliobrevin D (n = 5) or colchicine (n = 7) compared with nontreated cells (n = 6), calculated from midcell z section. Significance was determined by a one-way ANOVA. **, P < 0.001; ***, P < 0.0001. Error bars show mean and SEM.

(Lindman et al., 2018). In the current study, we investigated the mechanisms behind this microtubule-dependent regulation of Kv7.4 channels. Our data not only provide the first evidence of dynein influencing Kv7.4 channel trafficking but also show that this dynein-dependent process regulates vascular function and depends on cholesterol-rich caveolae.

In heterologous expression systems, dynein influences the expression of several potassium channels (Choi et al., 2005; Loewen et al., 2009); but none had investigated the Kv7 channel family. Given our previous findings (Lindman et al., 2018), we focused on the Kv7.4 channel, and similar to previous studies investigating the role of dynein on Kv channels, we adopted an

Table 1. Proteins identified following dynein immunoprecipitation, trypsin digestion, and liquid chromatography–tandem MS analysis

Protein	UniProt accession no.
Caveolae-associated protein 1	G3V8L9
Caveolin-1	Q2IBC6
Cytoplasmic dynein 1 heavy chain 1	F1LRT9
Cytoplasmic dynein 1 intermediate chain 2	D3ZU74

The identifications were based on at least two peptides matched confidently per protein in four of four replicates, which were absent in control samples from immunoprecipitations without IgG and in the presence of normal mouse control IgG.

electrophysiological approach. Both overexpression of p50/dynamitin, to interfere with dynein function, and ciliobrevin D, to inhibit the movement of dynein, increased the Kv7.4 current in HEK293B cells. In silico analysis of the Kv7.4 channel identified two dynein recognition sites in the C terminus of the channel. Mutating an exposed glutamine residue (580) confirmed dynein's ability to bind to this region, since the currents produced by this channel were larger than the Kv7.4 WT currents, increasing to a similar degree as ciliobrevin D treatment on the WT channel, and neither p50 overexpression nor ciliobrevin D treatment was able to increase the mutant Kv7.4 current density. Overexpression of p50 had a greater effect on the Kv7.4 current than ciliobrevin D treatment and the Kv7.4-Q580A mutation did. Coexpression of p50 is known to disrupt many dynein-dynactin–dependent processes. The exact mechanism of disruption is not completely clear but probably involves disruption of the dynein–dynactin interaction (Schroer, 2004). This disruption to the dynein–dynactin complex is known to alter dynein-dependent retrograde, as well as anterograde, transport of membrane proteins and multiple organelles by disrupting the binding of the dynein complex to its cargo (Burkhardt et al., 1997; Utrilla et al., 2017). Overall, such treatment can completely rearrange the organelles in the cells, including the Golgi, ER, and lysosomes (Burkhardt et al., 1997). With such a multitude of effects on cell function, it is not
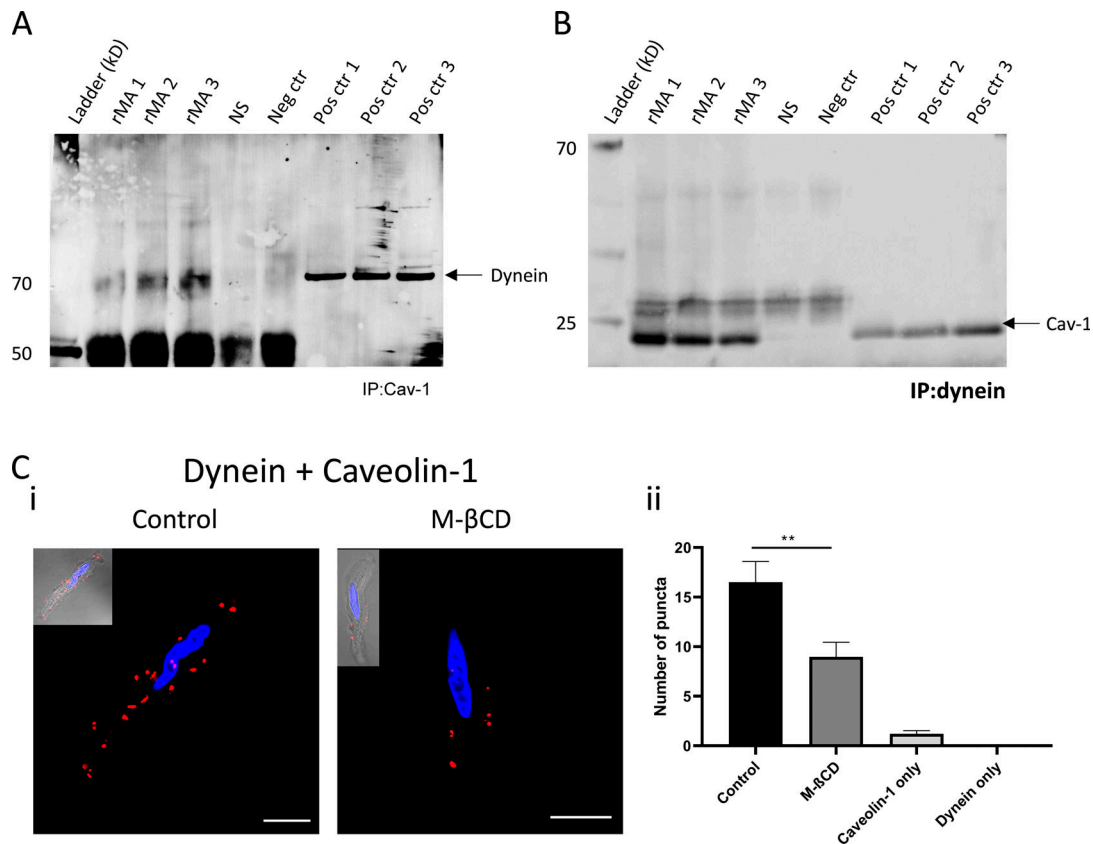

Figure 6. Dynein colocalizes with caveolin-1 proteins. (A) Representative dynein (∼74 kD) bands from a Western blot with rat mesenteric artery protein lysate (rMA) that was immunoprecipitated (IP) with a caveolin-1 (Cav-1) antibody (*n* = 3) and the total protein lysate as positive control. **(B)** Representative caveolin-1 (∼22 kD) bands from a Western blot with rMA that was immunoprecipitated with a dynein antibody (*n* = 3) and the total protein lysate as positive control. Each rMA sample contains *n* = 3 rats' worth of mesenteric arteries. No bands for dynein or Cav-1 were detected for the nonspecific binding sample (NS) or for the negative control sample (Neg ctr) where normal rabbit/mouse control IgG was used instead of the specific pulldown antibody. **(C i)** Representative images of PLA in smooth muscle cells from rat mesenteric arteries with dynein and caveolin-1 antibodies in control (left) and M-βCD–treated (right) cells. Red puncta indicate that target proteins are in close proximity (<40 nM). Scale bars, 10 µm. **(C ii)** Quantification of the number of PLA puncta in mesenteric artery myocytes (34 cells, *n* = 4 rats) showing significant decrease of dynein and caveolin-1 colocalization in M-βCD treated cells (**, P = 0.004 according to an unpaired *t* test). Error bars represent SEM.
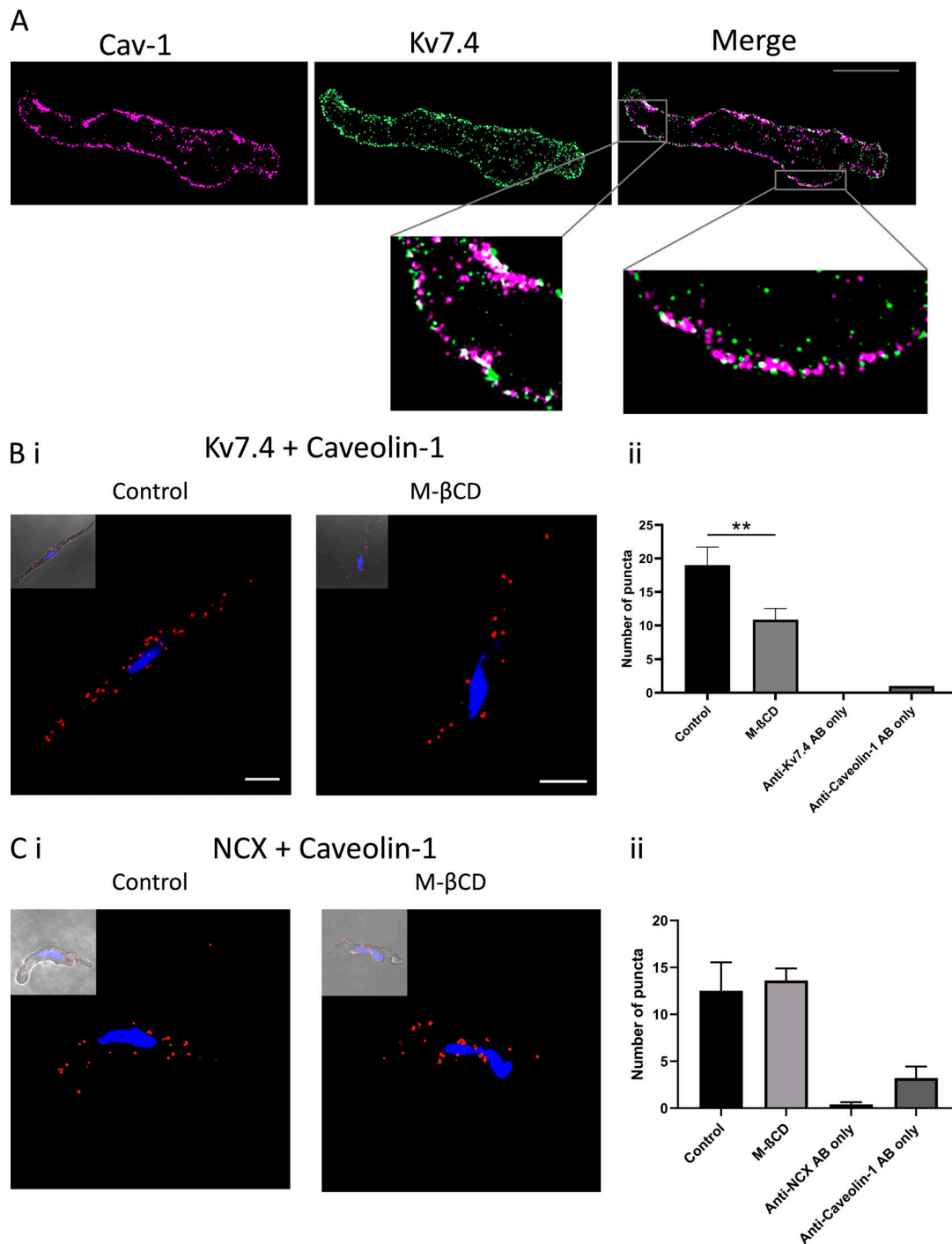
Figure 7. **Kv7.4 channels colocalize with caveolin-1. (A)** Representative midcell z section of an isolated smooth muscle cell from a rat small mesenteric artery stained with antibodies against caveolin-1 (Cav-1; magenta) and Kv7.4 (green). Scale bar, 10 μm. Insets show the brightfield images of the cells. **(B i)** Representative images of PLAs in smooth muscle cells from rat mesenteric arteries with Kv7.4 and caveolin-1 antibodies in control (left) and M-βCD–treated (right) cells. Red puncta indicate target proteins are in close proximity (<40 nM). **(B ii)** Quantification of the number of PLA puncta in mesenteric artery myocytes (control: 27 cells, n = 3 rats; M-βCD: 29 cells, n = 3 rats) showing significant decrease of Kv7.4 and caveolin-1 colocalization in M-βCD–treated cells (**, P = 0.008 according to an unpaired t test). **(C i)** Representative images of PLAs in smooth muscle cells from rat mesenteric arteries with NCX and caveolin-1 antibodies in control (left) and M-βCD–treated (right) cells. Red puncta indicate target proteins are in close proximity (<40 nM). **(C ii)** Quantification of the number of PLA puncta in mesenteric artery myocytes (control, 10 cells; M-βCD, 10 cells) showing equal colocalization of NCX and caveolin-1 in M-βCD–treated cells compared with nontreated cells. Error bars represent SEM.
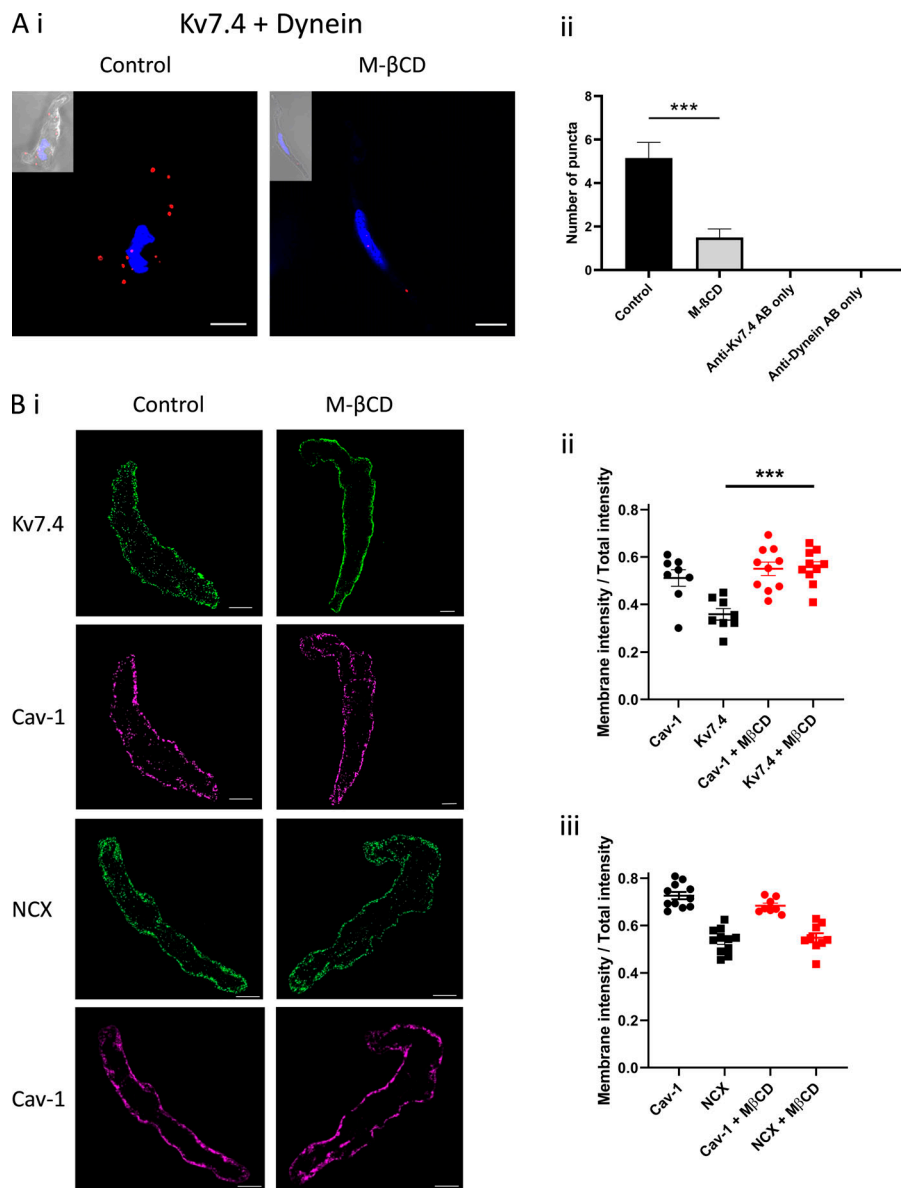
Figure 8. Dynein trafficking of Kv7.4 is dependent on cholesterol. (A i) Representative images of PLAs in smooth muscle cells from rat mesenteric arteries with Kv7.4 and dynein antibodies in control (left) and M-βCD–treated (right) cells. Red puncta indicate target proteins are in close proximity (<40 nM). Scale bars, 10 μm. **(A ii)** Quantification of the number of PLA puncta in mesenteric artery myocytes (control, 20 cells, *n* = 2 rats; M-βCD, 18 cells, *n* = 2 rats) showing significant decrease of Kv7.4 and caveolin-1 colocalization in M-βCD–treated cells (***, P < 0.0001 according to an unpaired *t* test). **(B i)** Representative midcell z section of a mesenteric artery myocyte treated with or without M-βCD and stained for caveolin-1 (Cav-1; magenta) and Kv7.4 or NCX (green). **(B ii)** Mean membrane intensity of Kv7.4 relative to total intensity in cells increased with M-βCD (*n* = 10) compared with nontreated control cells (*n* = 8; according to a one-way ANOVA. ***, P < 0.0001). Scale bars, 5 μm. **(B iii)** Mean membrane intensity of NCX relative to total intensity in cells was equal in M-βCD–treated cells (*n* = 10) and nontreated control cells (*n* = 9–11). The intensity of caveolin-1 was the same for both groups. Error bars show mean values and SEM.

possible, within the scope of this study, to determine why p50 overexpression had an enhanced effect on the WT Kv7.4 current compared with ciliobrevin D treatment and the Kv7.4-Q580A mutation. Nevertheless, these data highlight the importance of the dynein recognition sequence in the C terminus of Kv7.4 channels for dynein-dependent regulation since the Kv7.4-Q580A mutant was completely unaffected by p50 overexpression. Given that this glutamine residue is conserved throughout the Kv7 channel family, this dynein-dependent transport mechanism may be a common mechanism in several organs where these channels are also important physiologically, such as the heart, brain, pancreas, and smooth muscle cells.

One striking effect from our electrophysiological studies was the inhibition of the Kv7.4-Q580A currents by ciliobrevin D. To investigate this effect, we performed in silico docking experiments with the known structures for Kv7.1 and Kv7.4. These data showed that ciliobrevin D could bind to the mutant channel, but not the WT Kv7.1 or Kv7.4 channels, in an area important for

channel multimerization and trafficking from the ER (Howard et al., 2007; Haitin and Attali, 2008; Wiener et al., 2008). We propose, therefore, that the binding of ciliobrevin D to the mutant channel prevents the functional formation of Kv7.4 channels in the cell membrane, thereby inhibiting the current. Given this off-target effect of ciliobrevin D on the mutant Kv7.4 channel, it is not possible to interpret the effect of ciliobrevin D on the dynein-dependent regulation of the Kv7.4-Q580A channel.

It is well established that vascular voltage-gated Kv7 potassium channels are important regulators of arterial tone, with activation of the Kv7 channels hyperpolarizing the membrane, leading to a relaxation of the smooth muscle cells and concomitant vasodilatation (Zhong et al., 2010b; Ng et al., 2011; Jepps et al., 2014; Stott et al., 2014). Kv7.4 and Kv7.5 are the two predominant functional isoforms in vascular smooth muscle cells, where they mostly form heteromeric Kv7.4/7.5 channels (Brueggemann et al., 2014; Chadha et al., 2014; Jepps et al.,
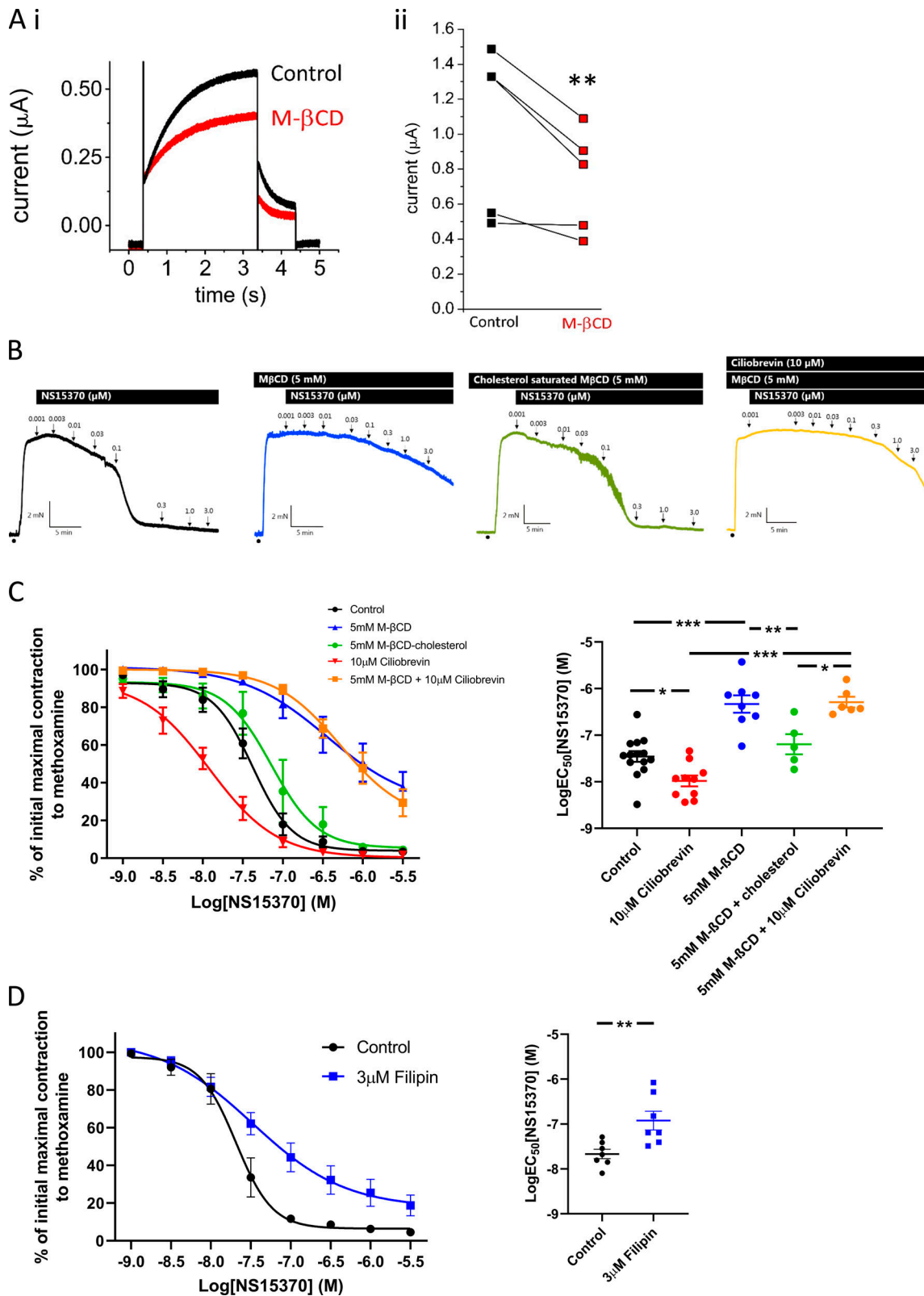
Figure 9. **Cholesterol depletion inhibits Kv7 channel function in mesenteric arteries. (A i)** Representative recording of a Kv7.4 current from a *Xenopus* oocyte before (black) and after (red) application of 1 mM M-βCD. **(A ii)** Mean data showing the effect of M-βCD on the Kv7.4 current in *Xenopus* oocytes at 40 mV (*n* = 5). **, P < 0.01 according to a paired *t* test. **(B)** Representative isometric tension recordings of rat mesenteric artery segments preconstricted with methoxamine (•) before sequentially increasing concentrations of Kv7.2–Kv7.5–specific activator NS15370 were applied in (from left to right) control, M-βCD–treated, cholesterol-saturated M-βCD–treated, and M-βCD + ciliobrevin D–treated arteries. **(C)** Mean concentration-effect curves and EC_{50} values for the Kv7.2–Kv7.5–specific activator NS15370 in isometric tension recordings from either segments of mesenteric artery treated with 5 mM M-βCD (blue, *n* = 8),

5 mM M-βCD supplemented with cholesterol (green, *n* = 5), 10 µM ciliobrevin D (red, *n* = 10), or 5 mM M-βCD + 10 µM ciliobrevin D (orange, *n* = 6) or from control vessels (black, *n* = 14) when methoxamine was used to preconstrict the artery segments. M-βCD significantly attenuates the relaxation for NS15370, while cholesterol-saturated M-βCD had no effect compared with control vessels. Ciliobrevin D was unable to enhance relaxation in M-βCD–treated vessels. **(D)** Mean concentration-effect curves and EC_{50} values for the Kv7.2–Kv7.5–specific activator NS15370 in isometric tension recordings from segments of mesenteric artery treated with 3 µM Filipin III. 3 µM Filipin III significantly attenuates relaxation for NS15370. Statistical comparisons on the mean EC_{50} values were performed with a one-way ANOVA followed by a Tukey multiple comparisons test. *, $P < 0.05$; **, $P < 0.001$; ***, $P < 0.0001$. Error bars show mean values and SEM.

2015). Therefore, we investigated whether the Kv7.4–dynein interaction observed in HEK293B cells was physiologically relevant in vascular smooth muscle.

Using PLA and coimmunoprecipitation assays, we identified dynein colocalization with Kv7.4 in isolated vascular smooth muscle cells and mesenteric artery lysate. Following this, we found that the relaxations to two different Kv7.2–Kv7.5 activators, S-1 and NS15370 (Jepps et al., 2014), were enhanced by dynein inhibition, suggesting an increase in Kv7 channel function. To test this interpretation, we knocked down Kv7.4 protein in mesenteric artery segments (Jepps et al., 2015). Since the targeted morpholino produced a knockdown of Kv7.4 by inserting a splice site, thereby rendering the expressed protein nonfunctional, we assessed successful knockdown using the functional myography responses. As such, there was no relaxation to S-1 following incubation with the Kv7.4-targeted morpholino. Dynein inhibition enhanced the S-1 response in control morpholino-transfected arteries but had no effect in arteries where Kv7.4 was knocked down. We confirmed that Kv7.4 protein was increased in the membrane of both mesenteric artery smooth muscle cells and HEK293B cells following ciliobrevin D treatment and used the expression of the NCX as a negative control for these experiments. These results confirm that dynein is involved in the removal of the channels from the cell membrane of vascular smooth muscle cells and that inhibition of dynein increases the number of Kv7.4 channels in the membrane, thereby increasing the functional impact of the channel in the arteries.

Since their discovery, ciliobrevin compounds have been used by several groups to investigate the functional roles of dynein (Eyre et al., 2014; Fu et al., 2014; Sikirzhytski et al., 2014; Cao et al., 2015); however, this is the first study to exploit these inhibitors to reveal a cardiovascular role for dynein. Although the use of such inhibitors can be complicated by off-target effects, our electrophysiological data show that ciliobrevin D can increase Kv7.4 channel currents, and our Kv7.4 morpholino data provide compelling evidence that the enhanced S-1 effects with ciliobrevin D arise from increased Kv7.4 channel function.

Although we identified a direct binding site for dynein on Kv7.4, blocking dynein function does not prevent endocytosis and recycling of early endosomes (Granger et al., 2014; Rezaul et al., 2016). Therefore, we speculated that the Kv7.4 protein was internalized in a vesicle that was targeted by dynein for removal away from the cell membrane, perhaps through binding to the Kv7.4 channel directly. We performed mass spectrometry on mesenteric artery protein lysates to investigate dynein-bound proteins that could comprise a functional vesicle in which the Kv7.4 protein was being trafficked. Strikingly, caveolae proteins were identified in the mass spectrometry experiments. We

confirmed the interaction of dynein with caveolin-1 by coimmunoprecipitation and PLA.

Caveolae are cholesterol-rich regions of the smooth muscle cell plasma membrane formed by membrane proteins called caveolins and cavins, in particular caveolin-1, which is essential for caveolae formation (Root et al., 2015; Parton et al., 2018). These flask-shaped plasma membrane microdomains (50–100 nm) are enriched in lipids such as cholesterol and sphingolipids, where cholesterol is the major component and is crucial for the structural integrity of the microdomain. Several membrane proteins localize in caveolae (Dart, 2010; Villar et al., 2016), and Kv7.1–Kv7.3 channels are known to localize in cholesterol-rich domains (Oldfield et al., 2009; Roura-Ferrer et al., 2010; Zhang et al., 2013; Oliveras et al., 2014; Delgado-Ramírez et al., 2018). Although caveolae provide important microdomains in the cell membrane, they are also internalized as motile vesicles important for the transport of certain proteins within or across polarized cells (Mundy et al., 2002). Several studies have shown that intracellular caveolae movement is regulated by microtubules, with disruption of the microtubule network increasing membrane expression of caveolae (Mundy et al., 2002; Tagawa et al., 2005; Head et al., 2006, 2014). Importantly, dynein motors cluster around cholesterol-rich microdomains in various cells types, which is thought to be an important regulatory mechanism for this motor, allowing it to function efficiently (Johansson et al., 2005; Rocha et al., 2009; Rai et al., 2016; Wijdeven et al., 2016).

Our data show that dynein and Kv7.4 proteins can interact with the caveolin-1 protein of caveolae. Depleting cholesterol in the cells reduced the number of interactions between Kv7.4 and dynein, as well as dynein interactions with caveolin-1. This depletion increased membrane localization of Kv7.4 proteins to a similar extent as ciliobrevin D treatment. In line with previous studies showing that dynein clusters to cholesterol-rich microdomains (Johansson et al., 2005; Rocha et al., 2009; Rai et al., 2016; Wijdeven et al., 2016), our data show that cholesterol is an integral component of this dynein-dependent trafficking mechanism. Thus, when Kv7.4 proteins are located in the cholesterol-rich caveolae, they can be targeted by dynein for retrograde trafficking from the membrane.

Since Kv7.4 membrane expression was enhanced after cholesterol depletion, we speculated that M-βCD would enhance Kv7.4 channel currents and Kv7-specific arterial relaxations to a similar extent as ciliobrevin D treatment did. Surprisingly, M-βCD inhibited currents arising from oocyte overexpression of Kv7.4, and in myography experiments, the relaxation to NS15370 was attenuated after cholesterol depletion with M-βCD. This effect was confirmed using the cholesterol-binding agent Filipin III. In addition, ciliobrevin D incubation had no effect on

the M-βCD–induced inhibition of NS15370 relaxation, suggesting that the inhibition was not related to cell tracking or the number of channel proteins in the plasma membrane and functionally confirming the need for cholesterol to target dynein-dependent trafficking of Kv7.4 channels. Previously, Kv7.2/7.3 channel activity was inhibited after cholesterol depletion (Delgado-Ramírez et al., 2018), and we suggest that vascular Kv7 channels require cholesterol and/or caveolae not only to be trafficked but also for correct function within the cell membrane. M-βCD has been used in several studies investigating smooth muscle function, where it has affected multiple ion channels and proteins (Löhn et al., 2000; Dreja et al., 2002; Smith et al., 2005; Morikage et al., 2006; Shmygol et al., 2007; Sones et al., 2010), which may also account for the reduced Kv7 channel function in our arterial preparations.

As the focus of this study was on understanding Kv7.4 trafficking, we have not characterized the implications of the dynein–caveolin-1 interaction further. In addition, the precise molecular interactions regulating dynein binding to the caveolae–Kv7.4 complex have not been investigated. For example, oxysterol-binding protein-related protein 1L (ORP1L) is a cholesterol-sensing switch essential for dynein tethering and the minus-end transport of certain vesicles (Johansson et al., 2005; Wijdeven et al., 2016; Rout et al., 2018). Investigating these proteins and their associations with dynein and Kv7.4 in smooth muscle cells may provide further insights into this trafficking mechanism. Finally, we have shown that despite increased membrane expression, cholesterol depletion inhibits the Kv7-dependent relaxation of arteries. One limitation of our study is the lack of whole-cell Kv7 currents from mesenteric artery smooth muscle cells; however, the direct inhibitory effect of M-βCD on Kv7.4 currents in oocytes, taken together with previous findings that Kv7.2/3 channels are inhibited by M-βCD (Delgado-Ramírez et al., 2018), is good evidence that Kv7.4 channels require cholesterol to function normally. Additional experiments are required to fully elucidate the role of cholesterol and the caveolae on Kv7.4 channel function.

The importance of caveolae in orchestrating signaling pathways is highlighted by their role in hypertension, where a reduction in the number of caveolae is a hallmark feature of arteries from hypertensive animals (Li et al., 2005; Albinsson et al., 2007; Rahman and Swärd, 2009; Swärd et al., 2013; Lian et al., 2019). Additionally, Kv7.4 channels are down-regulated and attenuated functionally in arteries from hypertensive animals (Jepps et al., 2011; Chadha et al., 2012). The results of this study indicate that future experiments should determine if the Kv7.4 down-regulation in arteries from hypertensive animals is associated with a reduced number of caveolae, with this possibly driven by a dysregulated microtubule network.

In summary, this study set out to determine if the microtubule-dependent regulation of Kv7.4 channels was through the dynein motor protein. We identified a dynein-binding domain in the C terminus of the Kv7.4 protein, which allows dynein to regulate Kv7.4 channel membrane expression. This interaction is relevant physiologically in vascular smooth muscle, where it is likely to underlie the microtubule-dependent regulation of Kv7.4 described previously (Lindman et al., 2018).

Furthermore, we have shown that dynein binds to caveolae proteins, where Kv7.4 channels appear to reside. Overall, this study provides the first evidence for a physiological role for dynein in vascular smooth muscles and outlines a complex regulatory trafficking mechanism for the Kv7.4 channel. Further work is required to fully understand the details of this association, as well as the potential role of other proteins regulated by dynein in smooth muscle cells.

References

Albinsson, S., Y. Shakirova, A. Rippe, M. Baumgarten, B.I. Rosengren, C. Rippe, R. Hallmann, P. Hellstrand, B. Rippe, and K. Swärd. 2007. Arterial remodeling and plasma volume expansion in caveolin-1-deficient mice. *Am. J. Physiol. Regul. Integr. Comp. Physiol.* 293:R1222–R1231. https://doi.org/10.1152/ajpregu.00092.2007

Barrese, V., J.B. Stott, S.N. Baldwin, G. Mondejar-Parreño, and L.A. Greenwood. 2020. SMIT (Sodium-Myo-Inositol Transporter) 1 Regulates Arterial Contractility Through the Modulation of Vascular Kv7 Channels. *Arterioscler. Thromb. Vasc. Biol.* 40:2468–2480.

Bentzen, B.H., N. Schmitt, K. Calloe, W. Dalby Brown, M. Grunnet, and S.-P. Olesen. 2006. The acrylamide (S)-1 differentially affects Kv7 (KCNQ) potassium channels. *Neuropharmacology.* 51:1068–1077. https://doi.org/10.1016/j.neuropharm.2006.07.001

Bhabha, G., G.T. Johnson, C.M. Schroeder, and R.D. Vale. 2016. How Dynein Moves Along Microtubules. *Trends Biochem. Sci.* 41:94–105. https://doi.org/10.1016/j.tibs.2015.11.004

Brueggemann, L.I., A.R. Mackie, L.L. Cribbs, J. Freda, A. Tripathi, M. Majetschak, and K.L. Byron. 2014. Differential protein kinase C-dependent modulation of Kv7.4 and Kv7.5 subunits of vascular Kv7

channels. *J. Biol. Chem.* 289:2099–2111. https://doi.org/10.1074/jbc.M113.527820

Burkhardt, J.K., C.J. Echeverri, T. Nilsson, and R.B. Vallee. 1997. Overexpression of the dynamitin (p50) subunit of the dynactin complex disrupts dynein-dependent maintenance of membrane organelle distribution. *J. Cell Biol.* 139:469–484. https://doi.org/10.1083/jcb.139.2.469

Cao, M., J. Ning, C.I. Hernandez-Lara, O. Belzile, Q. Wang, S.K. Dutcher, Y. Liu, and W.J. Snell. 2015. Uni-directional ciliary membrane protein trafficking by a cytoplasmic retrograde IFT motor and ciliary ectosome shedding. *eLife.* 4:e05242. https://doi.org/10.7554/eLife.05242

Chadha, P.S., F. Zunke, H.-L. Zhu, A.J. Davis, T.A. Jepps, S.P. Olesen, W.C. Cole, J.D. Moffatt, and I.A. Greenwood. 2012. Reduced KCNQ4-encoded voltage-dependent potassium channel activity underlies impaired β-adrenoceptor-mediated relaxation of renal arteries in hypertension. *Hypertension.* 59:877–884. https://doi.org/10.1161/HYPERTENSIONAHA.111.187427

Chadha, P.S., T.A. Jepps, G. Carr, J.B. Stott, H.-L. Zhu, W.C. Cole, and I.A. Greenwood. 2014. Contribution of kv7.4/kv7.5 heteromers to intrinsic and calcitonin gene-related peptide-induced cerebral reactivity. *Arterioscler. Thromb. Vasc. Biol.* 34:887–893. https://doi.org/10.1161/ATVBAHA.114.303405

Choi, W.S., A. Khurana, R. Mathur, V. Viswanathan, D.F. Steele, and D. Fedida. 2005. Kv1.5 surface expression is modulated by retrograde trafficking of newly endocytosed channels by the dynein motor. *Circ. Res.* 97:363–371. https://doi.org/10.1161/01.RES.0000179535.06458.f8

Dalby-Brown, W., C. Jessen, C. Hougaard, M.L. Jensen, T.A. Jacobsen, K.S. Nielsen, H.K. Erichsen, M. Grunnet, P.K. Ahring, P. Christophersen, et al. 2013. Characterization of a novel high-potency positive modulator of K(v)7 channels. *Eur. J. Pharmacol.* 709:52–63. https://doi.org/10.1016/j.ejphar.2013.03.039

Dart, C. 2010. Lipid microdomains and the regulation of ion channel function. *J. Physiol.* 588:3169–3178.

Delgado-Ramírez, M., S. Sánchez-Armass, U. Meza, and A.A. Rodríguez-Menchaca. 2018. Regulation of Kv7.2/Kv7.3 channels by cholesterol: Relevance of an optimum plasma membrane cholesterol content. *Biochim. Biophys. Acta Biomembr.* 1860:1242–1251. https://doi.org/10.1016/j.bbamem.2018.02.016

Dreja, K., M. Voldstedlund, J. Vinten, J. Tranum-Jensen, P. Hellstrand, and K. Swärd. 2002. Cholesterol depletion disrupts caveolae and differentially impairs agonist-induced arterial contraction. *Arterioscler. Thromb. Vasc. Biol.* 22:1267–1272. https://doi.org/10.1161/01.ATV.0000023438.32585.A1

Echeverri, C.J., B.M. Paschal, K.T. Vaughan, and R.B. Vallee. 1996. Molecular Characterization of the 50-kD Subunit of Dynactin Reveals Function for the Complex in Chromosome Alignment and Spindle Organization during Mitosis. *J. Cell Biol.* 132:617–633.

Eyre, N.S., G.N. Fiches, A.L. Aloia, K.J. Helbig, E.M. McCartney, C.S.P. McErlean, K. Li, A. Aggarwal, S.G. Turville, and M.R. Beard. 2014. Dynamic imaging of the hepatitis C virus NS5A protein during a productive infection. *J. Virol.* 88:3636–3652. https://doi.org/10.1128/JVI.02490-13

Firestone, A.J., J.S. Weinger, M. Maldonado, K. Barlan, L.D. Langston, M. O'Donnell, V.I. Gelfand, T.M. Kapoor, and J.K. Chen. 2012. Small-molecule inhibitors of the AAA+ ATPase motor cytoplasmic dynein. *Nature.* 484:125–129. https://doi.org/10.1038/nature10936

Franker, M.A.M., and C.C. Hoogenraad. 2013. Microtubule-based transport - basic mechanisms, traffic rules and role in neurological pathogenesis. *J. Cell Sci.* 126:2319–2329. https://doi.org/10.1242/jcs.115030

Fu, W., P. Asp, B. Canter, and B.D. Dynlacht. 2014. Primary cilia control hedgehog signaling during muscle differentiation and are deregulated in rhabdomyosarcoma. *Proc. Natl. Acad. Sci. USA.* 111:9151–9156. https://doi.org/10.1073/pnas.1323265111

Granger, E., G. McNee, V. Allan, and P. Woodman. 2014. The role of the cytoskeleton and molecular motors in endosomal dynamics. *Semin. Cell Dev. Biol.* 31:20–29. https://doi.org/10.1016/j.semcdb.2014.04.011

Grosdidier, A., V. Zoete, and O. Michielin. 2011a. Fast docking using the CHARMM force field with EADock DSS. *J. Comput. Chem.* 32:2149–2159. https://doi.org/10.1002/jcc.21797

Grosdidier, A., V. Zoete, and O. Michielin. 2011b. SwissDock, a protein-small molecule docking web service based on EADock DSS. *Nucleic Acids Res.* 39(suppl):W270–W277. https://doi.org/10.1093/nar/gkr366

Haitin, Y., and B. Attali. 2008. The C-terminus of Kv7 channels: a multifunctional module. *J. Physiol.* 586:1803–1810. https://doi.org/10.1113/jphysiol.2007.149187

Head, B.P., H.H. Patel, D.M. Roth, F. Murray, J.S. Swaney, I.R. Niesman, M.G. Farquhar, and P.A. Insel. 2006. Microtubules and actin microfilaments regulate lipid raft/caveolae localization of adenylyl cyclase signaling components. *J. Biol. Chem.* 281:26391–26399. https://doi.org/10.1074/jbc.M602577200

Head, B.P., H.H. Patel, and P.A. Insel. 2014. Interaction of membrane/lipid rafts with the cytoskeleton: impact on signaling and function: membrane/lipid rafts, mediators of cytoskeletal arrangement and cell signaling. *Biochim. Biophys. Acta.* 1838:532–545. https://doi.org/10.1016/j.bbamem.2013.07.018

Howard, R.J., K.A. Clark, J.M. Holton, and D.L. Minor Jr. 2007. Structural insight into KCNQ (Kv7) channel assembly and channelopathy. *Neuron.* 53:663–675. https://doi.org/10.1016/j.neuron.2007.02.010

Jepps, T.A., P.S. Chadha, A.J. Davis, M.I. Harhun, G.W. Cockerill, S.P. Olesen, R.S. Hansen, and I.A. Greenwood. 2011. Downregulation of Kv7.4 channel activity in primary and secondary hypertension. *Circulation.* 124:602–611. https://doi.org/10.1161/CIRCULATIONAHA.111.032136

Jepps, T.A., B.H. Bentzen, J.B. Stott, O.V. Povstyan, K. Sivaloganathan, W. Dalby-Brown, and A. Greenwood. 2014. Vasorelaxant effects of novel Kv7.4 channel enhancers ML213 and NS15370. *Br. J. Pharmacol.* 171:4413–4424.

Jepps, T.A., G. Carr, P.R. Lundegaard, S.-P. Olesen, and I.A. Greenwood. 2015. Fundamental role for the KCNE4 ancillary subunit in Kv7.4 regulation of arterial tone. *J. Physiol.* 593:5325–5340. https://doi.org/10.1113/JP271286

Johansson, M., M. Lehto, K. Tanhuanpää, T.L. Cover, and V.M. Olkkonen. 2005. The oxysterol-binding protein homologue ORP1L interacts with Rab7 and alters functional properties of late endocytic compartments. *Mol. Biol. Cell.* 16:5480–5492. https://doi.org/10.1091/mbc.e05-03-0189

Kilsdonk, E.P.C., P.G. Yancey, G.W. Stoudt, F.W. Bangerter, W.J. Johnson, M.C. Phillips, and G.H. Rothblat. 1995. Cellular cholesterol efflux mediated by cyclodextrins. *J. Biol. Chem.* 270:17250–17256. https://doi.org/10.1074/jbc.270.29.17250

Li, X.A., W.V. Everson, and E.J. Smart. 2005. Caveolae, lipid rafts, and vascular disease. *Trends Cardiovasc. Med.* 15:92–96. https://doi.org/10.1016/j.tcm.2005.04.001

Li, T., K. Wu, Z. Yue, Y. Wang, F. Zhang, and H. Shen. 2021. Structural Basis for the Modulation of Human KCNQ4 by Small-Molecule Drugs. *Mol. Cell.* 81:P25–P37.E4. https://doi.org/10.1016/j.molcel.2020.10.037

Lian, X., C. Matthaeus, M. Kaßmann, O. Daumke, and M. Gollasch. 2019. Pathophysiological Role of Caveolae in Hypertension. *Front. Med. (Lausanne).* 6:153. https://doi.org/10.3389/fmed.2019.00153

Lindman, J., M.M. Khammy, P.R. Lundegaard, C. Aalkjær, and T.A. Jepps. 2018. Microtubule Regulation of Kv7 Channels Orchestrates cAMP-Mediated Vasorelaxations in Rat Arterial Smooth Muscle. *Hypertension.* 71:336–345. https://doi.org/10.1161/HYPERTENSIONAHA.117.10152

Loewen, M.E., Z. Wang, J. Eldstrom, A. Dehghani Zadeh, A. Khurana, D.F. Steele, and D. Fedida. 2009. Shared requirement for dynein function and intact microtubule cytoskeleton for normal surface expression of cardiac potassium channels. *Am. J. Physiol. Heart Circ. Physiol.* 296: H71–H83. https://doi.org/10.1152/ajpheart.00260.2008

Löhn, M., M. Fürstenau, V. Sagach, M. Elger, W. Schulze, F.C. Luft, H. Haller, and M. Gollasch. 2000. Ignition of calcium sparks in arterial and cardiac muscle through caveolae. *Circ. Res.* 87:1034–1039. https://doi.org/10.1161/01.RES.87.11.1034

Morikage, N., H. Kishi, M. Sato, F. Guo, S. Shirao, T. Yano, M. Soma, K. Hamano, K. Esato, and S. Kobayashi. 2006. Cholesterol primes vascular smooth muscle to induce Ca2 sensitization mediated by a sphingosyl-phosphorylcholine-Rho-kinase pathway: possible role for membrane raft. *Circ. Res.* 99:299–306. https://doi.org/10.1161/01.RES.0000235877.33682.e9

Mulvany, M.J., and W. Halpern. 1977. Contractile properties of small arterial resistance vessels in spontaneously hypertensive and normotensive rats. *Circ. Res.* 41:19–26. https://doi.org/10.1161/01.RES.41.1.19

Mundy, D.I., T. Machleidt, Y.S. Ying, R.G.W. Anderson, and G.S. Bloom. 2002. Dual control of caveolar membrane traffic by microtubules and the actin cytoskeleton. *J. Cell Sci.* 115:4327–4339. https://doi.org/10.1242/jcs.00117

Ng, F.L., A.J. Davis, T.A. Jepps, M.I. Harhun, S.Y. Yeung, A. Wan, M. Reddy, D. Melville, A. Nardi, T.K. Khong, and I.A. Greenwood. 2011. Expression and function of the K+ channel KCNQ genes in human arteries. *Br. J. Pharmacol.* 162:42–53. https://doi.org/10.1111/j.1476-5381.2010.01027.x

Norman, A.W., R.A. Demel, B. DeKruyff, and L.M.M. van Deenen. 1972. Studies on the biological properties of polyene antibiotics. Evidence for the direct interaction of filipin with cholesterol. *J. Biol. Chem.* 247: 1918–1929. https://doi.org/10.1016/S0021-9258(19)45558-0

Oldfield, S., J. Hancock, A. Mason, S.A. Hobson, D. Wynick, E. Kelly, A.D. Randall, and N.V. Marrion. 2009. Receptor-mediated suppression of potassium currents requires colocalization within lipid rafts. *Mol. Pharmacol.* 76:1279–1289. https://doi.org/10.1124/mol.109.058008

Oliveras, A., M. Roura-Ferrer, L. Solé, A. de la Cruz, A. Prieto, A. Etxebarria, J. Manils, D. Morales-Cano, E. Condom, C. Soler, et al. 2014. Functional assembly of Kv7.1/Kv7.5 channels with emerging properties on vascular muscle physiology. *Arterioscler. Thromb. Vasc. Biol.* 34:1522–1530. https://doi.org/10.1161/ATVBAHA.114.303801

Parton, R.G., V.A. Tillu, and B.M. Collins. 2018. Caveolae. *Curr. Biol.* 28: R402–R405. https://doi.org/10.1016/j.cub.2017.11.075

Rahman, A., and K. Swärd. 2009. The role of caveolin-1 in cardiovascular regulation. *Acta Physiol. (Oxf.).* 195:231–245. https://doi.org/10.1111/j.1748-1716.2008.01907.x

Rai, A., D. Pathak, S. Thakur, S. Singh, A.K. Dubey, and R. Mallik. 2016. Dynein Clusters into Lipid Microdomains on Phagosomes to Drive Rapid Transport toward Lysosomes. *Cell.* 164:722–734. https://doi.org/10.1016/j.cell.2015.12.054

Rappsilber, J., Y. Ishihama, and M. Mann. 2003. Stop and go extraction tips for matrix-assisted laser desorption/ionization, nanoelectrospray, and LC/MS sample pretreatment in proteomics. *Anal. Chem.* 75:663–670. https://doi.org/10.1021/ac026117i

Rezaul, K., D. Gupta, I. Semenova, K. Ikeda, P. Kraikivski, J. Yu, A. Cowan, I. Zaliapin, and V. Rodionov. 2016. Engineered Tug-of-War Between Kinesin and Dynein Controls Direction of Microtubule Based Transport In Vivo. *Traffic.* 17:475–486. https://doi.org/10.1111/tra.12385

Rocha, N., C. Kuijl, R. van der Kant, L. Janssen, D. Houben, H. Janssen, W. Zwart, and J. Neefjes. 2009. Cholesterol sensor ORP1L contacts the ER protein VAP to control Rab7-RILP-p150 Glued and late endosome positioning. *J. Cell Biol.* 185:1209–1225. https://doi.org/10.1083/jcb.200811005

Rodríguez-Crespo, I., B. Yélamos, F. Roncal, J.P. Albar, P.R. Ortiz de Montellano, and F. Gavilanes. 2001. Identification of novel cellular proteins that bind to the LC8 dynein light chain using a pepscan technique. *FEBS Lett.* 503:135–141. https://doi.org/10.1016/S0014-5793(01)02718-1

Roossien, D.H., K.E. Miller, and G. Gallo. 2015. Ciliobrevins as tools for studying dynein motor function. *Front. Cell. Neurosci.* 9:252. https://doi.org/10.3389/fncel.2015.00252

Root, K.T., S.M. Plucinsky, and K.J. Glover. 2015. Recent progress in the topology, structure, and oligomerization of caveolin: a building block of caveolae. *Curr. Top. Membr.* 75:305–336. https://doi.org/10.1016/bs.ctm.2015.03.007

Roura-Ferrer, M., L. Solé, A. Oliveras, R. Dahan, J. Bielanska, A. Villarroel, N. Comes, and A. Felipe. 2010. Impact of KCNE subunits on KCNQ1 (Kv7.1) channel membrane surface targeting. *J. Cell. Physiol.* 225:692–700. https://doi.org/10.1002/jcp.22265

Rout, A.K., X. Wu, M.R. Starich, M.-P. Strub, J.A. Hammer, and N. Tjandra. 2018. The Structure of Melanoregulin Reveals a Role for Cholesterol Recognition in the Protein's Ability to Promote Dynein Function. *Structure.* 26:1373–1383.e4. https://doi.org/10.1016/j.str.2018.07.009

Schroer, T.A. 2004. Dynactin. *Annu. Rev. Cell Dev. Biol.* 20:759–779. https://doi.org/10.1146/annurev.cellbio.20.012103.094623

Shmygol, A., K. Noble, and S. Wray. 2007. Depletion of membrane cholesterol eliminates the Ca2+-activated component of outward potassium current and decreases membrane capacitance in rat uterine myocytes. *J. Physiol.* 581:445–456. https://doi.org/10.1113/jphysiol.2007.129452

Sievers, F., A. Wilm, D. Dineen, T.J. Gibson, K. Karplus, W. Li, R. Lopez, H. McWilliam, M. Remmert, J. Söding, et al. 2011. Fast, scalable generation of high-quality protein multiple sequence alignments using Clustal Omega. *Mol. Syst. Biol.* 7:539. https://doi.org/10.1038/msb.2011.75

Sikirzhytski, V., V. Magidson, J.B. Steinman, J. He, M. Le Berre, I. Tikhonenko, J.G. Ault, B.F. McEwen, J.K. Chen, H. Sui, et al. 2014. Direct kinetochore-spindle pole connections are not required for chromosome segregation. *J. Cell Biol.* 206:231–243. https://doi.org/10.1083/jcb.201401090

Smith, R.D., E.B. Babiychuk, K. Noble, A. Draeger, and S. Wray. 2005. Increased cholesterol decreases uterine activity: functional effects of cholesterol alteration in pregnant rat myometrium. *Am. J. Physiol. Cell Physiol.* 288:C982–C988. https://doi.org/10.1152/ajpcell.00120.2004

Sones, W.R., A.J. Davis, N. Leblanc, and I.A. Greenwood. 2010. Cholesterol depletion alters amplitude and pharmacology of vascular calcium-activated chloride channels. *Cardiovasc. Res.* 87:476–484. https://doi.org/10.1093/cvr/cvq057

Steele, D.F., and D. Fedida. 2014. Cytoskeletal roles in cardiac ion channel expression. *Biochim. Biophys. Acta.* 1838:665–673. https://doi.org/10.1016/j.bbamem.2013.05.001

Stott, J.B., T.A. Jepps, and I.A. Greenwood. 2014. K(V)7 potassium channels: a new therapeutic target in smooth muscle cells. *Drug Discov. Today.* 19:413–424. https://doi.org/10.1016/j.drudis.2013.12.003

Stott, J.B., V. Barrese, and I.A. Greenwood. 2016. Kv7 Channel Activation Underpins EPAC-Dependent Relaxations of Rat Arteries. *Arterioscler. Thromb. Vasc. Biol.* 36:2404–2411. https://doi.org/10.1161/ATVBAHA.116.308517

Stott, J.B., V. Barrese, M. Suresh, S. Masoodi, and I.A. Greenwood. 2018. Investigating the role of G protein βγ in Kv7-dependent relaxations of the rat vasculature. *Arterioscler. Thromb. Vasc. Biol.* 38:2091–2102. https://doi.org/10.1161/ATVBAHA.118.311360

Sun, J., and R. MacKinnon. 2017. Cryo-EM Structure of a KCNQ1/CaM Complex Reveals Insights into Congenital Long QT Syndrome. *Cell.* 169: 1042–1050.e9. https://doi.org/10.1016/j.cell.2017.05.019

Sun, J., and R. MacKinnon. 2020. Structural Basis of Human KCNQ1 Modulation and Gating. *Cell.* 180:340–347.e9. https://doi.org/10.1016/j.cell.2019.12.003

Swärd, K., M.K. Sadegh, M. Mori, J.S. Erjefält, and C. Rippe. 2013. Elevated pulmonary arterial pressure and altered expression of Ddah1 and Arg1 in mice lacking cavin-1/PTRF. *Physiol. Rep.* 1:1–10. https://doi.org/10.1002/PHY2.8

Tagawa, A., A. Mezzacasa, A. Hayer, A. Longatti, L. Pelkmans, and A. Helenius. 2005. Assembly and trafficking of caveolar domains in the cell: caveolae as stable, cargo-triggered, vesicular transporters. *J. Cell Biol.* 170:769–779. https://doi.org/10.1083/jcb.200506103

Utrilla, R.G., P. Nieto-Marín, S. Alfayate, D. Tinaquero, M. Matamoros, M. Pérez-Hernández, S. Sacristán, L. Ondo, R. de Andrés, F.J. Díez-Guerra, et al. 2017. Kir2.1-Nav1.5 channel complexes are differently regulated than Kir2.1 and Nav1.5 channels alone. *Front. Physiol.* 8:903. https://doi.org/10.3389/fphys.2017.00903

van der Horst, J., I.A. Greenwood, and T.A. Jepps. 2020. Cyclic AMP-Dependent Regulation of Kv7 Voltage-Gated Potassium Channels. *Front. Physiol.* 11:727. https://doi.org/10.3389/fphys.2020.00727

Villar, V.A.M., S. Cuevas, X. Zheng, and P.A. Jose. 2016. Localization and signaling of GPCRs in lipid rafts. *Methods Cell Biol.* 132:3–23. https://doi.org/10.1016/bs.mcb.2015.11.008

Wiener, R., Y. Haitin, L. Shamgar, M.C. Fernández-Alonso, A. Martos, O. Chomsky-Hecht, G. Rivas, B. Attali, and J.A. Hirsch. 2008. The KCNQ1 (Kv7.1) COOH terminus, a multitiered scaffold for subunit assembly and protein interaction. *J. Biol. Chem.* 283:5815–5830. https://doi.org/10.1074/jbc.M707541200

Wijdeven, R.H., H. Janssen, L. Nahidiazar, L. Janssen, K. Jalink, I. Berlin, and J. Neefjes. 2016. Cholesterol and ORP1L-mediated ER contact sites control autophagosome transport and fusion with the endocytic pathway. *Nat. Commun.* 7:11808. https://doi.org/10.1038/ncomms11808

Wiśniewski, J.R., A. Zougman, N. Nagaraj, and M. Mann. 2009. Universal sample preparation method for proteome analysis. *Nat. Methods.* 6: 359–362. https://doi.org/10.1038/nmeth.1322

Zhang, H., Y. Liu, J. Xu, F. Zhang, H. Liang, X. Du, and H. Zhang. 2013. Membrane microdomain determines the specificity of receptor-mediated modulation of Kv7/M potassium currents. *Neuroscience.* 254: 70–79. https://doi.org/10.1016/j.neuroscience.2013.08.064

Zhong, X.Z., K.S. Abd-Elrahman, C.-H. Liao, A.F. El-Yazbi, E.J. Walsh, M.P. Walsh, and W.C. Cole. 2010a. Stromatoxin-sensitive, heteromultimeric Kv2.1/Kv9.3 channels contribute to myogenic control of cerebral arterial diameter. *J. Physiol.* 588:4519–4537. https://doi.org/10.1113/jphysiol.2010.196618

Zhong, X.Z., M.I. Harhun, S.P. Olesen, S. Ohya, J.D. Moffatt, W.C. Cole, and I.A. Greenwood. 2010b. Participation of KCNQ (Kv7) potassium channels in myogenic control of cerebral arterial diameter. *J. Physiol.* 588: 3277–3293. https://doi.org/10.1113/jphysiol.2010.192823